ChemComm

Cite this: *Chem. Commun.*, 2012, **48**, 11813–11831

www.rsc.org/chemcomm

FEATURE ARTICLE

Microporous metal–organic frameworks for storage and separation of small hydrocarbons

Yabing He,[a] Wei Zhou,[bc] Rajamani Krishna[d] and Banglin Chen*[a]

Received 26th July 2012, Accepted 27th September 2012
DOI: 10.1039/c2cc35418g

Hydrocarbons are very important energy resources and raw materials for some industrially important products and fine chemicals. There is a need for the discovery of better materials that offer enhanced capacities for safe storage of hydrocarbons. Furthermore, the development of improved separation technologies will lead to significant reduction in energy requirements and costs. In this feature article, we provide an overview of the current status of the emerging microporous metal–organic frameworks for the storage and separation of small hydrocarbons.

1. Introduction

The inorganic solid state chemistry and crystal engineering community has witnessed the emergence and growth of the porous metal–organic framework (MOF) materials over the past two decades.[1,2] This new type of porous materials can be readily self-assembled from their corresponding metal ions and/or metal-containing clusters with suitable organic linkers. The richness of metal ions and organic linkers has enabled us to synthesize a large number of porous MOFs of diverse structures and/or topologies whose pore dimensions can be systematically varied from ultramicro- to meso-porous domains by the interplay of metal-containing secondary building units and organic linkers. Furthermore, the pore surfaces within MOF materials can be functionalized through the immobilization of functional organic groups such as $-NH_2$, –OH, and $-SO_3H$, and open (unsaturated) metal sites to direct their specific recognition of molecules and substrates, and thus to target their multifunctionalities and applications in gas storage,[3] separation,[4] catalysis,[5] molecular recognition,[6] drug delivery,[7] proton conductivity,[8] and so on.

The term "metal–organic framework" was coined by Yaghi in 1995 to describe the first two MOF materials that exhibited unique properties for ion exchange, and selective binding and removal of guest molecules, respectively.[9] This term has been widely utilized after the realization of the prototypic **MOF-5** whose BET surface area is over 3000 $m^2\ g^{-1}$.[10] Apparently, metal–organic frameworks are closely related to coordination polymers (CPs);[11] however, MOFs distinguish themselves from CPs through their unique structural flexibility and/or

[a] *Department of Chemistry, University of Texas at San Antonio, One UTSA Circle, San Antonio, Texas 78249-0698, USA. E-mail: Banglin.Chen@utsa.edu; Fax: +1-210-458-7428; Tel: +1-210-458-5461*
[b] *NIST Center for Neutron Research, Gaithersburg, Maryland 20899-6102, USA*
[c] *Department of Materials Science and Engineering, University of Maryland, College Park, Maryland 20742, USA*
[d] *Van't Hoff Institute of Molecular Science, University of Amsterdam, Science Park 904, 1098 XH Amsterdam, The Netherlands*

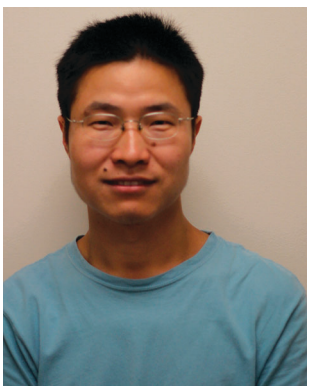

Yabing He

Yabing He earned his PhD in organic chemistry from Changchun Institute of Applied Chemistry, Chinese Academy of Sciences, under the direction of Prof. Lianxun Gao in 2010. Currently, he works with Prof. Banglin Chen at the University of Texas at San Antonio as a postdoctoral fellow. His current research focuses on the design and synthesis of porous materials and study of their hydrocarbon adsorption and separation properties.

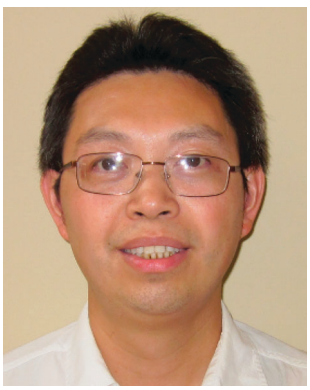

Wei Zhou

Wei Zhou received his PhD in 2005 from the University of Pennsylvania, under the supervision of Prof. John E. Fischer. From 2005 to 2007, he was a post-doctoral researcher at the NIST Center for Neutron Research (NCNR), working with Dr Taner Yildirim. After that, he was appointed to his current position as a research scientist at NCNR and the University of Maryland. His research interests are in the areas of novel porous materials, computational materials design, and neutron spectroscopy.

Table 1 Physical–chemical properties of small hydrocarbons

Hydrocarbon	Mp[a] [K]	Bp[b] [K]	T_c[c] [K]	P_c[d] [MPa]	ΔH_{vap}[e] [kJ mol^{-1}]	α[f] $\times 10^{25}$ [cm^3]	μ[g] $\times 10^{18}$ [esu cm]	Θ[h] $\times 10^{26}$ [esu cm^2]	σ[i] [Å]
Methane	90.6	111.6	190.5	4.596	8.18	25.93	0	0	3.758
Acetylene	189.1	189.3	308.3	6.191	20.87	33.3–39.3	0	—	3.3
Ethylene	103.9	169.4	282.6	5.076	13.54	42.52	0	1.50	4.163
Ethane	89.8	184.4	305.4	4.884	14.69	44.3–44.7	0	0.65	4.443
Propyne	170	250	402.3	5.628					
Propylene	87.8	225.4	364.2	4.610	18.42	62.6	0.366	—	4.678
Propane	85.4	231.1	369.8	4.250	18.75	62.9–63.7	0.084	—	4.3–5.118
n-Butane	133	272.6	425.1	3.796	22.41	82.0	0.05	—	4.687
iso-Butane	40–240	261.4	408.1	3.648		81.4–82.9	0.132	—	5.278
1-Butene	87.7	266.9	419.5	4.020	21.91	79.7–85.2	0.359–0.438	—	4.5
iso-Butene	132.9	266	417.8	4.001	22.46				
cis-2-Butene	134.3	276.8	435.5	4.207	23.34	—	0.253	—	4.23
trans-2-Butene	167.7	274	428.1	4.080	22.74	84.9	0	—	
1-Pentene	108	303							
cis-2-Pentene	93	310–311							
trans-2-Pentene	133	310							
n-hexane	177–179	341.6–342.2	507.6	3.025		119	0		4.3
3mp[j]	155.15	336.4	504.4	3.120					5.0
22dmb[k]	171–175	322.87	488.7	3.080					6.2

[a] Melting point. [b] Boiling point. [c] Critical temperature. [d] Critical pressure. [e] Heat of vaporization (101.3 kPa at boiling point). [f] Polarizability. [g] Dipole moment. [h] Quadrupole moment. [i] Kinetic diameter. [j] 3-Methylpentane. [k] 2,2-Dimethylbutane.

robustness and then eventual permanent porosities. The main motivation to term "metal–organic frameworks" might be to feature their similarity with the traditional framework solids, particularly zeolite framework materials, and thus to emphasize their permanent porosities. In our view, metal–organic frameworks can be defined as the two- and three-dimensional framework materials that are self-assembled from metal ions and/or metal-containing clusters with organic linkers whose permanent porosities can be established by vapor–gas sorption isotherms. Obviously, the term "coordination polymers" is much broader than "metal–organic frameworks". To some extent, porous coordination polymers are basically the same as metal–organic frameworks.

Small hydrocarbons play a vital role in the chemical and petroleum industries due to their utilization as fuels or raw materials. Their physical–chemical properties are given in Table 1. Methane, the principal component of natural gas, is a clean alternative to other automobile fuels such as gasoline and diesel. Ethane and propane are the important chemicals for the production of corresponding ethylene and propylene through industrial scale cracking processes. Acetylene is widely used as a fuel and a chemical building block for synthesis of various fine chemicals. Ethylene and propylene are used as monomer feedstock in the production of polyethylene and polypropylene. Realization of safe and high-capacity storage and efficient separation of these small hydrocarbons will certainly promote their wide applications. In this feature article, we will highlight the recent progress in the development of porous metal–organic frameworks for their storage and separation.

2. CH_4 storage in porous MOFs

Air quality is a major public health concern, especially in urban areas. The use of clean fuels for vehicular applications is thus strongly encouraged. Natural gas (NG) is a valuable

Rajamani Krishna

Rajamani Krishna received his PhD degree in Chemical Engineering from the University of Manchester (1975). He has been involved in a wide range of process development research activities within the Shell group of companies (The Netherlands), and later as Director of the Indian Institute of Petroleum. Since 1990, Krishna has been Professor at the University of Amsterdam with current research focus on adsorption and diffusion in porous materials, membrane separation, and pressure swing adsorption. He has published three textbooks on diffusion, has more than 400 peer-reviewed publications, and holds several patents. Currently, his h-index is 53.

Banglin Chen

Banglin Chen was born in Zhejiang, China. He received BS (1985) and MS (1988) degrees in Chemistry from Zhejiang University in China, and PhD from National University of Singapore in 2000. He worked with Professors Omar M. Yaghi at University of Michigan, Stephen Lee at Cornell University and Andrew W. Maverick at Louisiana State University as a postdoctoral fellow during 2000–2003 before joining the University of Texas-Pan American in 2003. He moved to the University of Texas at San Antonio in August 2009, and now he is the Professor of Chemistry.

alternative fuel due to its relative abundance and clean-burning characteristics in comparison with conventional fuels such as gasoline and diesel. However, the energy density of NG per unit volume is as low as just 0.11% of that of gasoline. Therefore, for large scale use, it is necessary to store natural gas in a safe and economical way. Three main storage methods have been proposed: (a) liquefied natural gas (LNG); (b) compressed natural gas (CNG); and (c) adsorbed natural gas (ANG). LNG is obtained by cryogenic techniques and stored as boiling liquid at 112 K and 100 kPa. The need for expensive cryogenic tanks together with boil-off losses have prevented its widespread commercial applications, especially for small vehicles. CNG is stored as supercritical fluid at room temperature and 20–30 MPa by using steel cylinders. The whole process is also costly since it requires multistage compression. Adsorbed natural gas (ANG) storage is a booming technology for natural gas storage. The studies on the storage by the ANG method are mainly carried out using methane, the primary constituent of the natural gas. Until now various adsorbents including zeolites and porous carbon materials have been studied for methane adsorption. MOFs owing to their large surface areas, well-defined pore sizes and tailorable structures are fast becoming materials to reckon with in this field.[12]

To promote the vehicular application of methane, in 2000, the US Department of Energy (DOE) has set the performance target for methane storage of 180 V(STP)/V (standard temperature and pressure equivalent volume of methane per volume of the adsorbent material) at 3.5 MPa and 298 K.[13] In terms of energy density, this volumetric storage capacity is comparable to methane compressed at 25 MPa (298 K). In addition, the methane adsorbent should also have low adsorption heat, high heat capacity, high packing density, high mechanical stability, quantitative NG desorption, low affinity for strong adsorbing species, and reasonable cost.[14]

The first report on methane uptake by a porous MOF dates back to as early as 1997 as pioneered by Kitagawa and co-workers.[15] The reported coordination polymer $[Co_2(4,4'\text{-bpy})_3(NO_3)_4]$ adsorbs very limited but encouraging methane of 52 $cm^3\ g^{-1}$ (71 $cm^3\ cm^{-3}$) at 298 K and 3.0 MPa. Subsequently, several interpenetrated coordination compounds were constructed using the longer bridging ligand 4,4′-azopyridine (azpy).[16] Despite the framework interpenetration, the networks still contain the microporous channels capable of taking up methane gas with the highest of the series only adsorbing 40 $cm^3\ g^{-1}$ (62 $cm^3\ cm^{-3}$) at 3.6 MPa and 298 K. Methane adsorption properties were also investigated in three isotypic pillared-layer porous materials.[17] They are composed of the two-dimensional sheets of Cu(pzdc) linked together by different pillar ligands such as pyrazine, 4,4′-bipyridine, and *N*-(pyridin-4-yl)isonicotinamide (pia), respectively. The channel sizes and chemical environments are varied systematically, thus resulting in different methane uptake values ranging from 19 to 67 $cm^3\ g^{-1}$ at 298 K and 3.5 MPa. The methane adsorption experiments were also carried out on a three-dimensional coordination polymer $[CuSiF_6(4,4'\text{-bpy})_2]$.[18] The three-dimensional network consists of two-dimensional sheets of $Cu(4,4'\text{-bpy})_2$ pillared by SiF_6 anions. The methane adsorption quantity reaches 146 $cm^3\ g^{-1}$ (125 $cm^3\ cm^{-3}$) at 298 K and 3.6 MPa. This is the first MOF with methane adsorption capacity surpassing zeolite 5A (83 $cm^3\ g^{-1}$).

In 2001, Seki *et al*. systematically investigated the methane adsorption properties in a series of highly porous pillared-layer MOFs $Cu_2(L)_2(ted)$ (L = fma, bdc, sdc, or bpdc).[19] The compounds are composed of dicopper paddle-wheel units bridged by four dicarboxylates to two-dimensional square-grid layers. The axial sites of the paddle-wheels are coordinated by nitrogen atoms of the neutral TED ligands, connecting the 2D layers into a 3D structure with a primitive cubic net topology. Using the short tripod-shaped ted as a pillar ligand can effectively prevent framework catenation, resulting in noninterpenetrated structures with high porosity. When a longer pillar ligand 4,4′-bipyridine was used instead of ted, a flexible two-fold interpenetrated coordination polymer $Cu_2(bdc)_2(4,4'\text{-bpy})$ was formed.[20] Of these compounds investigated, $Cu_2(sdc)_2(ted)$ possesses the highest methane adsorption capacity of 213 $cm^3\ g^{-1}$ at 298 K and 3.5 MPa. This value is much higher than that of zeolite 5A and nearly the same as that of the high-surface-area activated carbon AX-21.[21] It should be mentioned that $Cu_2(bdc)_2(ted)$, $Zn_2(bdc)_2(ted)$,[22] and $Co_2(bdc)_2(ted)$[23] exhibit slightly different methane uptake although they are isostructural, suggesting that different metal identity has also a certain effect on the methane adsorption capacity in this system.

IRMOF-6 is one member of isoreticular metal–organic frameworks (IRMOF) reported by Yaghi's group in 2002, with the composition of $Zn_4O(L)_3$ (L = benzocyclobutane-3,6-dicarboxylate), exhibiting an exceptionally high methane storage capacity of 240 $cm^3\ g^{-1}$ (155 $cm^3\ cm^{-3}$) at 298 K and 3.6 MPa, significantly higher than other MOFs at that time.[24] Such high methane uptake may be attributed to the high accessible surface area and the functionality of the ligand. Inspired by this result, computer simulations were performed by Snurr *et al*., and they predicted that **IRMOF-993** (L = 9,10-anthracene dicarboxylate), an artificially constructed but until now not synthesized material, could have better volumetric methane storage capacity (181 $cm^3\ cm^{-3}$) than **IRMOF-6**.[25] Attempts to synthesize this proposed MOF, however, resulted in an ultramicroporous material with very limited methane uptake.[26]

After these early encouraging research studies, several copper-carboxylate MOFs were examined for high-pressure methane adsorption. Regarding their topology, most of them can be grouped into the following two categories. One is (4,4)-connected NbO-type structure like **PCN-11**,[27] **PCN-14**,[28] **PCN-16/16′**,[29] **PCN-46**,[30] and **NOTT-107**.[31] They are constructed by the self-assembly of di-isophthalate ligands and dicopper paddle-wheel secondary building units. Of these materials, **PCN-14**, based on an anthracene derivative 5,5′-(9,10-anthracenediyl)-diisophthalate (adip), stands out in terms of its exceptionally high excess methane storage capacity of 220 $cm^3\ cm^{-3}$ at 290 K and 3.6 MPa, which is 22% higher than the DOE target for methane storage. Nanoscopic cages with the size suitable for methane storage and accessible open copper sites within this porous MOF are responsible for such high methane storage (Fig. 1). Also, the heats of adsorption of methane at low loadings are as high as 30 kJ mol^{-1}. Both the methane-adsorption capacity and the initial heat of adsorption are the highest reported thus far. Another category of copper-carboxylate MOFs possesses (3,24)-connected net structure with the organic linkers incorporating hexacarboxylate groups. Examples include **PCN-61**, **PCN-66**, **PCN-68**, and **NOTT-119**.[32,33] The use of this network

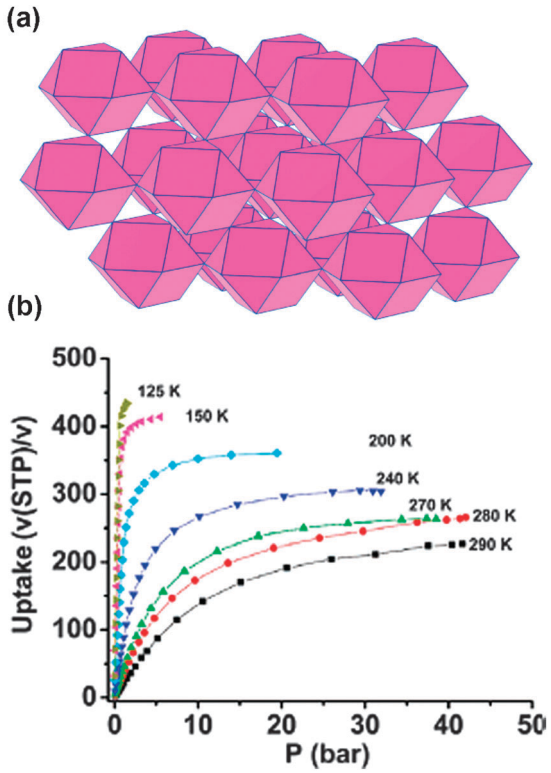

Fig. 1 (a) Nanoscopic cages in **PCN-14**. (b) High-pressure excess methane adsorption isotherms of **PCN-14** at various temperatures. Reprinted with permission from ref. 28. Copyright 2008, American Chemical Society.

topology can effectively eschew framework interpenetration, and create hierarchical pore cages, and upon desolvation, generate accessible open metal sites, which are favorable for high-pressure gas storage. The saturated gravimetric methane adsorption capacities correlate well with their gravimetric surface areas/pore volumes; however, the volumetric methane uptake capacities do not follow the trend due to their different crystal density. Therefore, to achieve high volumetric methane uptake capacity, a balance should be maintained among porosity, density, pore size and other factors.

To investigate the role of open metal sites in methane adsorption, in 2009, Zhou and co-workers studied methane adsorption in a series of **MOF-74-M** materials (M = Mg, Mn, Co, Ni, Zn), which possess high concentrations of open metal sites.[2h] The methane adsorption isotherm measurements at 298 K and 3.5 MPa for the five **MOF-74-M** materials yielded excess methane storage capacities ranging from 149 to 190 $cm^3\ cm^{-3}$. Among the five isostructural MOFs investigated, **NiMOF-74** exhibited the highest excess methane storage capacity of 190 $cm^3\ cm^{-3}$. This is the second MOF material whose excess methane adsorption capacity has potentially exceeded the DOE target. The neutron diffraction experiments reveal that the open metal sites are the primary methane adsorption sites and play a major role in the adsorption of methane. Furthermore, the study on the influence of MOF shaping on methane storage properties of **NiMOF-74** was performed by Tagliabue *et al.*[34] Shaping is an essential step for industrial implementation of MOFs in methane storage. The shaped sample obtained by compacting **NiMOF-74** at 0.1 GPa exhibits a slight lower methane uptake at 303 K and 3.5 MPa (129 $cm^3\ g^{-1}$) than the as-synthesized one (157 $cm^3\ g^{-1}$). Considering the particle density of 0.78 g cm^{-3}, the shaped sample only adsorbs about 100 $cm^3\ cm^{-3}$ of methane, which is approximately half of what an ideal single crystal sample would adsorb volumetrically.

Recently, our research group reported a new copper-carboxylate MOF **UTSA-20** of a novel **zyg** topology, with the excess volumetric methane storage capacity of 178 $cm^3\ cm^{-3}$ at 300 K and 3.5 MPa, which is the third porous MOF whose excess volumetric methane storage is very close to the DOE methane storage target.[35] **UTSA-20** was formed by the self-assembly of a noncoplanar hexacarboxylate organic linker H_6bhb (H_6bhb = 3,3′,3″,5,5′,5″-benzene-1,3,5-triyl-hexabenzoic acid) with the dicopper paddle-wheel $Cu_2(COO)_4$ SBU. There exist 1D rectangular pores of about 3.4 Å × 4.8 Å and 1D cylinders of 8.5 Å in diameter along the *c* axis (Fig. 2a). Computational investigations indicate that besides the open copper site, the linker channel site is also one of primary methane adsorption sites, and that the methane binding at the linker channel sites is even stronger than that at the open copper sites because the methane molecule is well sandwiched between two bhb linker potential surfaces. The methane storage density of 0.222 g cm^{-3} in micropores in **UTSA-20** at 300 K and 3.5 MPa is equivalent to the density of compressed methane at 300 K and 34 MPa. Such high methane storage density is attributed to the full utilization of both open copper sites and the pore spaces.

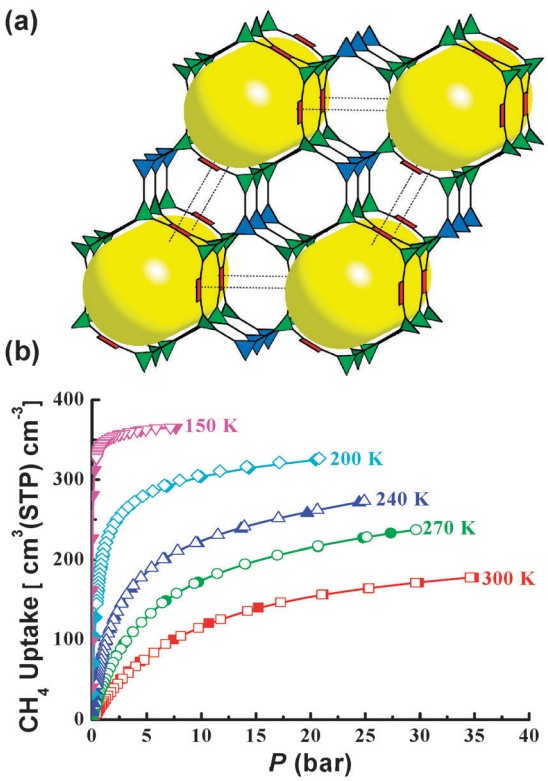

Fig. 2 (a) The pore structure of **UTSA-20** along the *c* axis. (b) High-pressure excess methane sorption isotherms of **UTSA-20** at various temperatures. Reprinted with permission from ref. 35. Copyright 2011, Wiley.

The characterization of the methane sorption sites within porous MOFs is conducive to understanding the gas sorption mechanism and thus to further developing MOF materials with higher methane sorption capacity. X-ray single-crystal diffraction and neutron powder diffraction are two valuable tools for identifying the gas adsorption sites within MOFs at low temperatures.[36] Using high-resolution neutron powder diffraction in combination with computational methods, Zhou and co-workers investigated the methane binding sites within **HKUST-1**, **PCN-11**, and **PCN-14**.[37] These MOFs contain two types of unique surface sites that can strongly interact with methane molecules. One is the coordinatively unsaturated metal ions, and the other is the enhanced vdW potential pockets. The open metal ions can bind methane strongly through a Coulomb-type electrostatic interaction, while at the vdW potential pocket sites, the methane molecules interact with multiple surfaces, leading to an overall enhanced dispersive interaction. The existence of various strong adsorption sites is fully responsible for the high methane uptake found in these MOF materials. Kim *et al.* determined the methane adsorption sites in $Zn_2(bdc)_2(dabco)$ using X-ray single-crystal diffraction.[22a] The crystal structure analysis of methane-loaded $Zn_2(bdc)_2$-(dabco) revealed three independent methane sorption sites in its cavities. They are located near the $Zn_2(COO)_4$ paddle wheel units, near the center of the small windows, and at the center of the cavity, respectively. These sorption sites correspond to a sorption stoichiometry of $Zn_2(bdc)_2(dabco)\cdot 6.69CH_4$, which is consistent with the gas sorption measurements at 198 K. Methane adsorption behavior in a series of IRMOFs was investigated using Raman spectroscopy at room temperature and high pressure,[38] conditions that are relevant to storage systems. The studies have revealed that methane adsorption is clearly not dominated by the metal clusters and the organic linkers play the critical roles in the adsorption behavior of gases in these MOFs.

In Table 2, we summarise the surface area, porosity and methane uptake data for the reported porous MOFs. It can be seen that the excess methane storage performances of a few MOFs have potentially surpassed the DOE target. It should be emphasized that the volumetric storage capacities reported were calculated directly from the measured gravimetric values using the crystal density. Considering that the material bulk density is much less than the crystal density due to the void generated by particle packing, the real v/v value of the bulk MOF material would be significantly smaller than that reported. To achieve the DOE target in terms of system performance, the volumetric methane uptake based on MOF crystal density has to be significantly higher than the DOE target.

Of the thousands of MOFs reported so far, only a small fraction has been examined for their methane adsorption properties. To identify existing MOFs whose methane storage potentials were not previously recognized, or to synthesize new MOFs particularly targeted for methane storage application, some general guidelines are needed. Recently, Snurr's group performed systematically Grand Canonical Monte Carlo (GCMC) computer simulations on methane adsorption in a large number ($>100\,000$) of hypothetical MOFs.[31] Their work not only identified many new hypothetical MOFs that may exhibit higher methane uptake than those of the currently known MOFs, but also identified several important structure–property relationships. For example, the volumetric methane uptake was found to correlate with the volumetric surface area quite well. In terms of the much more widely used gravimetric surface area, the optimal range is 2500–3000 $m^2\ g^{-1}$, going past which only worsens the volumetric methane storage capacity. Similarly, for the pore fraction (*i.e.*, how porous is the MOF), there exists an optimal value, which is ~ 0.8. In terms of pore size, the optimal values are ~ 4 and ~ 8 Å, exactly enough for one or two methane molecules, although earlier work suggested that when the delivery is taken into account, the pore size of the adsorbent should be at least 11.4 Å (thickness of three methane molecules). These general structure–property relationships would certainly facilitate the discovery of new MOFs for methane storage applications in the near future.

3. C_2H_2 storage in porous MOFs

Acetylene is widely used as a fuel, and is a very important raw material for the synthesis of various fine chemicals. It is well known that acetylene is an unstable, highly reactive hydrocarbon. Pure acetylene under high pressure can react in an addition-type reaction to form products such as benzene and/or vinylacetylene. These reactions are exothermic so that vessels of acetylene stored at pressure above 0.2 MPa risk exploding at room temperature, even in the absence of oxygen. Thus, acetylene storage is very challenging. The current method of storing acetylene involves dissolution of the gas in acetone placed in a steel cylinder along with an absorbent. The volatile solvent contamination restricts its use in fine chemical products and electric materials. Also, acetylene can be stored using microporous materials such as zeolites and carbons, which can however catalyze C_2H_2 polymerization. Therefore, it is highly desired to discover new materials for its safe storage, transportation and delivery. As a class of newly emerging porous materials, metal–organic frameworks are likely the potential candidates to solve these issues due to the modular nature of the framework, which can be readily tailored synthetically or post-synthetically to reach the desirable sorption properties.[4e] Until now, several dozens of porous MOFs have been examined for their acetylene storage, which are summarized in Table 3.

Kitagawa and co-workers firstly reported the adsorption of acetylene in a microporous metal–organic material $Cu_2(pzdc)_2$-(pyz).[68] $Cu_2(pzdc)_2(pyz)$ has one-dimensional channels along the *a* axis with a cross-section of 4 Å × 6 Å, and there exist non-coordinated basic oxygen atoms on the pore surfaces as functional sites. It can take up C_2H_2 of 42 $cm^3\ g^{-1}$ (STP) at room temperature and 1 atm. The structure of C_2H_2-adsorbed $Cu_2(pzdc)_2(pyz)$ was determined by a maximum entropy method/Rietveld analysis using synchrotron X-ray diffraction data. In channels, the acetylene molecules are held at a periodic distance from one another by hydrogen bonding between two non-coordinated oxygen atoms in the nanoscale pore walls and the two hydrogen atoms of the acetylene molecules (Fig. 3). This permits the stable storage of acetylene at a density 200 times the safe compression limit of free acetylene at room temperature.

Table 2 The high-pressure methane sorption data for the reported porous MOFs

Materials	S_{BET} [$m^2\ g^{-1}$]	$S_{Langmuir}$ [$m^2\ g^{-1}$]	V_p[a] [$cm^3\ g^{-1}$]	D_c[b] [$g\ cm^{-3}$]	d[c] [$g\ cm^{-3}$]	CH_4 uptake[d] [$cm^3\ g^{-1}$] ([$cm^3\ cm^{-3}$])	ΔH_{ads}[e] [$kJ\ mol^{-1}$]	Ref.
$Co_2(4,4'\text{-bpy})_3(NO_3)_4$				1.364	—	54 (74)		15
$Cu_2(pzdc)_2(pyz)$				1.745		19 (33)		17
$Cu_2(pzdc)_2(4,4'\text{-bpy})$						57		17
$Cu_2(pzdc)_2(pia)$						67		17
$Co_2(azpy)_3(NO_3)_4$				1.316		13 (17)		16
$Co(azpy)_2(NCS)_2$				1.308		14 (19)		16
$Cd_2(azpy)_3(NO_3)_4$				1.539		42 (64)		16
$Cu(SiF_6)(4,4'\text{-bpy})_2$	1337		0.56	0.859	0.19	146 (125)		18*a*
$Cu(GeF_6)(4,4'\text{-bpy})_2$				0.925		134 (124)		18*b*
$Cu_2(PF_6)(NO_3)(4,4'\text{-bpy})_4{\cdot}1.4PF_6{\cdot}0.6NO_3$	559			1.057		31 (33)		18*b*
$Cu(dhbc)_2(4,4'\text{-bpy})$		320				70		39
Cu(bdc)	545	708	0.22			71		40
Cu(fma)	416	557	0.17			82		40
Cu(cdc)	347	456	0.15			60		40
$Cu_2(fma)_2(ted)$	606		0.23			104		19*c*
$Cu_2(bdc)_2(ted)$	1891		0.71	0.827	0.19	185 (153)		19*c*
$Cu_2(sdc)_2(ted)$	3129		1.07			213		19*a*,19*c*
$Cu_2(bpdc)_2(ted)$	3265		1.18			212		18*a*,19*c*
$Cu_2(bdc)_2(4,4'\text{-bpy})$	700		0.26			79		20
IRMOF-1	3800		1.04	0.593	0.16	227 (135)		24
IRMOF-3				0.634		189 (120)		24
IRMOF-6		2630	0.92	0.650	0.19	240 (155)		24
PCN-11	1931	2442	0.91	0.749	0.18	228 (171)	14.6	27
PCN-14	1753	2176	0.87	0.871	0.21	252 (220)[f]	30.0	28
PCN-16	2273	2800	1.06	0.724	0.15	220 (159)		29
PCN-16′	1760	2200	0.84	0.764	0.10	119 (91)		29
PCN-46	2500	2800	1.01	0.619	0.17	243 (150)		30
PCN-61	3000	3500	1.36	0.560	0.14	259 (145)		32
PCN-66	4000	4600	1.63	0.450	0.11	244 (110)		32
PCN-68	5109	6033	2.13	0.380	0.09	261 (99)		32
PCN-80	3850	4150	1.47	0.574	0.10	206 (118)		41
NOTT-107	1770					(171)		31
NOTT-119	4118		2.35	0.361	0.07	216 (78)		33
NOTT-140	2620		1.07	0.678	0.14	214 (145)[g]	16.6	42
DUT-4	1308	1996	0.68	0.773	0.14	136 (105)		43
DUT-5	1613	2335	0.81	0.634	0.13	153 (97)		43
DUT-6			2.02	0.386	0.07	203 (79)		44
DUT-8(Cu)	2535		1.04	0.680	0.12	181 (124)		45
DUT-8(Co)	1400		0.62	0.669	0.07	58 (39)		45
DUT-8(Zn)	710		0.30	0.677	0.11	48 (32)		45
DUT-9-SCD			1.77	0.467	0.08	187 (87)		46
DUT-13			1.98	0.385	0.07	184 (71)		47
DUT-23(Co)	4850		2.03	0.403	0.09	267 (108)		48
MOF-200	4530	10400	3.59	0.220	0.04	182 (40)		49
MOF-205	4460	6170	2.16	0.380	0.08	242 (92)		49
MOF-210	6240	10400	3.60	0.250	0.04	212 (53)		49
MgMOF-74	1332		0.61	0.909	0.19	164 (149)	18.5	2*h*
MnMOF-74	1102		0.50	1.084	0.21	146 (158)	19.1	2*h*
CoMOF-74	1056		0.48	1.169	0.22	149 (174)	19.6	2*h*
NiMOF-74	1027		0.44	1.206	0.26	158 (190)	20.2	2*h*
ZnMOF-74	885		0.41	1.231	0.24	139 (171)	18.3	2*h*
MIL-53(Cr)	1144	1500		1.040		159 (165)	17.0	50
MIL-53(Al)	1235	1627	0.54			(186)		51
MIL-100		2700	1.0			(119)	19.0	52
MIL-101c	2693	4492	1.30	0.310	0.17	313 (97)	18.0	22*b*,52
UTSA-20	1156	1783	0.63	0.910	0.22	196 (178)	17.7	35
UTSA-34b	991	1533	0.54	0.840	0.22	168 (141)[f]	20.0	53
UTSA-38a	1090	1690	0.61	0.962	0.15	131 (127)	18.9	54
SNU-30′	704	770	0.28	0.381	0.16	63 (24)		55
SNU-50′	2300	2450	1.08	0.650	0.18	267 (173)	26.8	56
SNU-70′	5290	6100	2.17	0.408	0.07	200 (82)	9.4	57
SNU-71′	1770	1923	0.71	0.835	0.13	131 (109)	14.6	57
SNU-77H	3670	4180	1.52	0.586	0.09	200 (117)	14.3	58
HKUST-1	1502	2216	0.76	0.880	0.19	200 (176)		22*b*
ZIF-8	1630	1810		0.924		98 (91)	12.0	59
$Co_2(bdc)_2(ted)$	1600	2300	0.82	0.815	0.15	171 (139)		23*a*
$Zn_2(bdc)_2(ted)$	1450		0.68	0.821	0.18	167 (137)	13.6	22*a*
Cd(bpydb)	346		0.35	1.430	0.15	75 (108)		60
$Zn_4O(fma)_3$	1120	1618	0.59	0.813	0.14	118 (96)[h]	12.0	61

Table 2 (*continued*)

Materials	S_{BET} [$m^2\ g^{-1}$]	$S_{Langmuir}$ [$m^2\ g^{-1}$]	V_p[a] [$cm^3\ g^{-1}$]	D_c[b] [$g\ cm^{-3}$]	d[c] [$g\ cm^{-3}$]	CH_4 uptake[d] [$cm^3\ g^{-1}$] ([$cm^3\ cm^{-3}$])	ΔH_{ads}[e] [$kJ\ mol^{-1}$]	Ref.
$Zn_9O_3(2,7\text{-ndc})_6$	901	1281	0.46	1.076	0.17	106 (114)		62
$Ni_2(2,6\text{-ndc})_2(ted)$	2307	2647	0.84	0.789	0.14	164 (129)	13.8	63
$Zn_6(btb)_4(4,4'\text{-bpy})_3$	4043	4624	1.43	0.405	0.11	226 (92)		64
$[Zn_3(OH)]_4(tbcppm)(H_2tbcppm)_2$	2718	3120	1.14	0.676	0.15	247 (167)		65
$Cu_3(tptc)_2(dabco)$	2703	3154	1.13	0.603	0.10[i]	164 (99)[i]		66
$Cu_3(tdpat)$	1938	2608	0.93	0.782	0.18[j]	231 (181)[j]		67
SDU-6	2826		1.17	0.611	0.15	242 (148)		128
SDU-7	2713		1.10	0.606	0.15	226 (137)		128
SDU-8	2516		1.02	0.639	0.14	196 (125)		128

[a] Pore volume. [b] Crystal density calculated from the single crystal structure without the guest molecules and terminal ligands and assuming no structural change of the framework. [c] Density of adsorbed methane in micropores. [d] Excess, at ambient temperature and 3.5 MPa. [e] Isosteric heat of adsorption at low coverage. [f] 290 K. [g] 293 K and 2.0 MPa. [h] 300 K and 3.0 MPa. [i] 298 K and 2.0 MPa. [j] Absolute.

Table 3 Acetylene adsorption on various porous MOFs at room temperature and atmospheric pressure

Material	S_{BET} ($S_{Langmuir}$) [$m^2\ g^{-1}$]	V_p[a] [$cm^3\ g^{-1}$]	D_c[b] [$g\ cm^{-3}$]	C_2H_2 uptake [$cm^3\ g^{-1}$] ([$cm^3\ cm^{-3}$])	d[c] [$g\ cm^{-3}$]	P[d] [MPa]	$-\Delta H$[e] [$kJ\ mol^{-1}$]	Ref.
$Cu_2(pzdc)_2(pyz)$	571		1.745	42(74)	0.09	8.1	42.5	68
$Mg(HCO_2)_2$	284	0.14	1.390	66(91)	0.11	10.1	38.5	70
$Mn(HCO_2)_2$	297	0.13	1.650	51(85)	0.10	9.3	38.5	70
$Cu_2(bdc)_2(dabco)$	—	0.73	0.820	60(49)	0.06	5.4	23.5	69
$Cu_2(ndc)_2(dabco)$	—	0.44	0.970	97(94)	0.11	10.4	27.5	69
$Cu_2(adc)_2(dabco)$	—	0.28	1.140	82(93)	0.11	10.3	33.7	69
$Zn_2(bdc)_2(dabco)$	—	0.75	0.830	93(77)	0.09	8.5	24.0	69
$Zn_2(ndc)_2(dabco)$	—	0.52	0.970	106(103)	0.12	11.4	30.3	69
$Zn_2(adc)_2(dabco)$	—	0.31	1.150	101(116)	0.13	12.8	36.2	69
1-$Cu_2(bpz)$	(660)	0.25	1.365	58(79)	0.09	8.7	32.0	75
1-$Ag_2(bpz)$	(600)	0.22	1.594	44(70)	0.08	7.7	28.4	75
Cu(etz)	—	—	1.177	70(82)	0.10	9.1	33.7	2*g*
HKUST-1	1401(2095)	0.76	0.879	201(177)	0.21	19.3	30.4	71
MOF-505	1139(1694)	—	0.927	148(137)	0.16	15.0	24.7	71
MOF-508	(946)	—	1.243	90(112)	0.13	12.2	—	71
MIL-53	816(1233)	—	0.928	72(67)	0.08	7.3	19.2	71
MOF-5	2381(3610)	—	0.590	26(15)	0.02	1.6	16.5	71
ZIF-8	1112(1758)	—	0.924	25(23)	0.03	2.5	13.3	71
CoMOF-74	1018(1504)	—	1.169	197(230)	0.27	25.1	50.1	73
MnMOF-74	695(993)	—	1.085	168(182)	0.21	19.8	39.0	73
MgMOF-74	927(1364)	—	0.909	184(167)	0.19	18.2	34.0	73
ZnMOF-74	747(1100)	—	1.231	122(150)	0.17	16.4	24.0	73
FeMOF-74	1350	0.63	1.126	156(176)[f]	0.20	19.4	47.0	76
UMCM-150	(3330)	1.21	0.636	129(82)	0.09	9.1	40.4	77
PCN-16	(2810)	1.00	0.718	176(126)	0.15	14.0	44.2	77
NOTT-101	(2930)	1.05	0.684	184(126)	0.15	13.9	37.1	77
NOTT-102	(3590)	1.28	0.587	146(86)	0.10	9.5		77
UTSA-20	(1894)	0.67	0.910	150(136)	0.16	15.1	30.8	77
UTSA-33a	660(1024)	0.37	0.993	84(83)	0.10	9.2	33.9	78
UTSA-34b	991(1532)	0.54	0.840	121(102)	0.12	11.2	50.0	53
UTSA-35a	743(758)	0.31	1.046	65(68)	0.08	7.5	29.5	79
UTSA-36a	495(806)	0.33	1.009	57(57)	0.07	6.4	29.0	80
UTSA-38a	1090(1690)	0.61	0.962	64(62)	0.07	6.8	24.7	54
$Cu_2(ebtc)$	1852(2844)	1.00	0.718	160(115)	0.13	12.7	34.5	81
$Zn_5(bta)_6(tda)_2$	414(607)	0.23	1.250	44(55)	0.06	6.1	37.3	82
$Zn_4(OH)_2(1,2,4\text{-btc})_2$	408	0.22	1.465	53(78)	0.09	8.6	28.2	83
Cu(bdc-OH)(4,4′-bpy)	553(761)	0.28	0.867	35(30)	0.04	3.4	39.5	84
Cu(bdc-OH)	397(584)	0.21	0.847	43(36)	0.04	4.0	25.7	85
Cu_4L[g]	1115(1722)	0.61	0.833	154(128)	0.15	14.2	—	86
Yb(bpt)	516(798)	0.29	0.986	24(24)	0.03	2.6	30.4	87

[a] Pore volume. [b] Crystal density calculated from the single-crystal structure without guest molecules and terminal ligands. [c] Density of adsorbed acetylene in bulk material. [d] Pressure of acetylene at 295 K corresponding to the calculated density of adsorbed acetylene in bulk material. [e] Isosteric heats of adsorption at low coverage. [f] 318 K. [g] H_8L = tetrakis[(3,5-dicarboxyphenoxy)methyl]methane.

Kitagawa also systematically investigated the acetylene sorption in six jungle-gym-like porous coordination polymers $[M_2(L)_2(dabco)]$ (M = Cu or Zn, L = bdc, 1,4-ndc, or adc) whose pore sizes and surface properties can be systematically tuned by changing the bridging dicarboxylate ligands.[69] Of these porous crystals, $Zn_2(adc)_2(dabco)$ has the highest

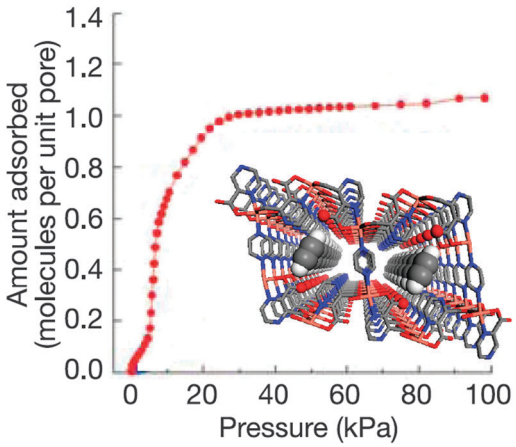

Fig. 3 C_2H_2 adsorption isotherm of $Cu_2(pzdc)_2(pyz)$ at 300 K. Inset: the crystal structure of C_2H_2-contained $Cu_2(pzdc)_2(pyz)$. Acetylene molecules: CPK model; non-coordinated oxygen atoms: ball and stick model. Hydrogen atoms except for those of acetylene are omitted for clarity. Reprinted with permission from ref. 68. Copyright 2005, Nature.

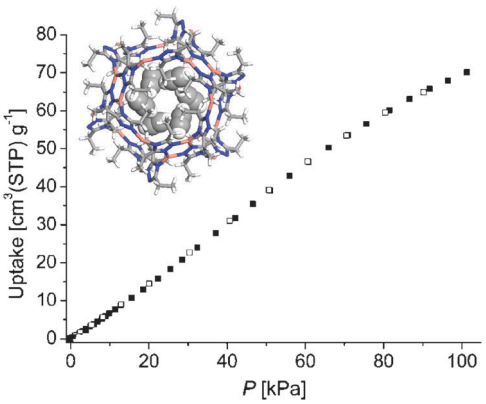

Fig. 4 C_2H_2 sorption isotherm of $[Cu(etz)]_n$ at 298 K. The filled and open symbols represent adsorption and desorption, respectively. Inset: the hexameric arrangement of acetylene molecules within the cage of $[Cu(etz)]_n$. Acetylene molecules: CPK model. Reprinted with permission from ref. 2*g*. Copyright 2009, American Chemical Society.

acetylene adsorption capacity and shows the highest affinity for acetylene. Such high affinity of $Zn_2(adc)_2(dabco)$ for acetylene is attributed not only to the micropore effect but also to acetylene–anthracene interactions because of the larger polarizability of anthracene than that of benzene or naphthalene.

Kim *et al.* studied the acetylene sorption in microporous manganese and magnesium formates that contain one-dimensional zigzag channels with a pore opening of 4.9 and 4.7 Å, respectively.[70] The amounts of adsorbed acetylene at 298 K and 1 atm are 65.7 and 51.2 cm^3 g^{-1} for $Mg(HCO_2)_2$ and $Mn(HCO_2)_2$, respectively. The X-ray crystal-structure analysis of acetylene-adsorbed metal formates shows that the acetylene molecules occupy two independent positions in the zigzag channels of the frameworks with a stoichiometry of $M(HCO_2)_2{\cdot}1/3C_2H_2$ or four molecules per unit cell. The shortest distances between the H atoms of C_2H_2 and the O atoms of the frameworks are in the range of 2.51–2.66 Å, which is close to the sum of the van der Waals radii of H and O atoms (2.6 Å). Obviously, there is no specific interaction except for van der Waals interactions between adsorbed acetylene molecules and the framework wall, as a result of which, the acetylene molecules are effectively held in the twisted narrow channels of Mg and Mn formates.

Zhang *et al.* studied the acetylene sorption in a dynamic porous crystal $[Cu(etz)]_n$.[2g] $[Cu(etz)]_n$ consists of a flexible NbO-type cuprous triazolate scaffold and a bcu pore system with large cavities interconnected by small, dynamic apertures. Although the host structure is seemingly impermeable, the highly flexible ethyl groups would allow the gas to diffuse into the pore even at extremely low adsorbate pressures. At 298 K and 1 atm, it can take up 70 cm^3 g^{-1} of C_2H_2. X-ray crystal structure analysis of C_2H_2-loaded $[Cu(etz)]_n$ indicates that the strongest host–guest interactions are C–H$\cdots$N contacts (C$\cdots$N = 3.44 and 3.47 Å) between C_2H_2 and the 1,2-nitrogens of etz, the most electronegative part of $[Cu(etz)]_n$. As the pocket is not deep enough, part of the C_2H_2 resides outside the pocket. The outer ends of six C_2H_2 molecules interact with each other by C–H$\cdots$C contacts (C$\cdots$C = 3.69 Å) in a *T*-shaped conformation to form an unprecedented S_6 cyclic hexamer (Fig. 4). It was speculated that the gas molecules should first enter the pores and then induce framework deformation and restrict framework motions. Such framework dynamics results in the sigmoid C_2H_2 isotherm.

Previous efforts on the MOFs for acetylene storage have mainly focused on those with small pores to enhance their acetylene adsorption enthalpies because the adsorption potential becomes deeper with decreasing pore width, which has however limited their uptake capacities with the highest ever reported being 106 cm^3 g^{-1}.[69] Thus, frameworks exhibiting both a deep adsorption potential and a large pore volume are desired to facilitate acetylene adsorption at ambient temperature.

Realizing that the open metal sites play a very important role in gas storage, our research group has examined six prototype microporous MOFs for acetylene storage, namely **HKUST-1**, **MOF-505**, **MOF-508**, **MIL-53**, **MOF-5**, and **ZIF-8**.[71] They can be classified into three types of pore structures featuring open metal sites (**HKUST-1** and **MOF-505**), small pores (**MOF-508** and **MIL-53**), and large pores (**MOF-5** and **ZIF-8**), respectively. Those with large pores (**MOF-5** and **ZIF-8**) are not favorable for acetylene storage. Those with small pores (**MOF-508** and **MIL-53**) take up a moderate amount of acetylene. **MOF-508** exhibits hysteretic sorption behavior due to the open-dense framework transformation.[72] Most remarkably, **HKUST-1** and **MOF-505** with open copper sites take up a significantly large amount of acetylene. The neutron powder diffraction studies demonstrate that the first and second strongest acetylene binding sites within **HKUST-1** are the open copper sites and the cage window sites, respectively, which are responsible for the exceptionally high acetylene uptake of 201 cm^3 g^{-1} (177 cm^3 cm^{-3}) at room temperature and 1 atm (Fig. 5a and b). The exceptionally high acetylene storage capacity of **HKUST-1** at room temperature and atmosphere pressure highlights the great promise of the immobilization of open metal sites to target some useful microporous MOF materials as practical acetylene storage media.

In searching for other MOFs with high-density open metal sites, we notice that the isostructural series **MOF-74** (also known as **CPO-27**, M_2(dhtp), M_2(dobdc)) have much higher densities of open metal sites (7.13–7.58 mmol cm^{-3})

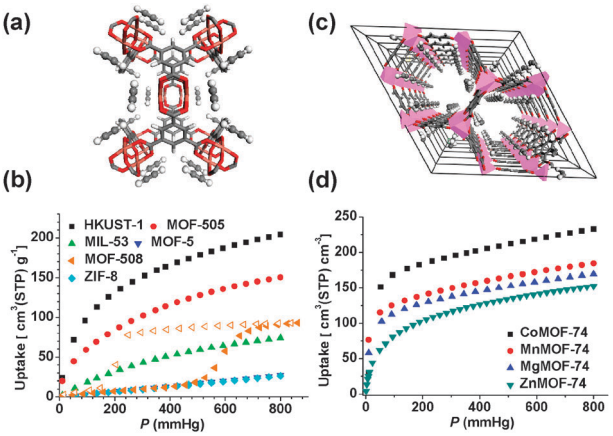

Fig. 5 (a) The crystal structure of one C_2D_2 per Cu loaded **HKUST-1** exhibiting the open copper sites for the recognition of acetylene molecules. (b) Acetylene adsorption isotherms of microporous MOFs at 295 K (**MOF-508** at 290 K). Solid symbols: adsorption; open symbols: desorption. (c) The crystal structure of 0.54 C_2D_2 per Co loaded **CoMOF-74** along the *c* axis exhibiting the high density of adsorbed acetylene molecules in pseudo-one-dimensional arrays. (d) C_2H_2 adsorption isotherms of **MOF-74-M** (M = Co, Mn, Mg, and Zn) at 295 K.

than **HKUST-1** (4.36 mmol cm^{-3}). These materials have one-dimensional hexagonal channels of ~11–12 Å in diameter. By examining these MOF series (M = Co, Mn, Mg, Zn), we realized **CoMOF-74** as the highest volumetric acetylene storage material ever reported with the uptake of 230 cm^3 cm^{-3} at 295 K and 1 atm (Fig. 5d).[73] The open metal sites within this series of isostructural MOFs exhibit differential interaction with acetylene molecules in which Co^{2+} has the strongest interactions with acetylene molecules. Neutron diffraction studies of C_2D_2-loaded **CoMOF-74** evidenced the open Co^{2+} sites as the preferential adsorption sites (Fig. 5c), which was further confirmed by the first-principle calculations. It should be mentioned that **NiMOF-74** exhibits significantly decayed adsorption of acetylene, which was further investigated in detail by Chavan *et al.*[74] The strongest binding of acetylene within **NiMOF-74** can be associated to the strong polarizing centers provided by **NiMOF-74** due to the small ionic radius of Ni^{2+} (83 pm) but does not lead to C_2H_2 polymerization under low-pressure conditions.

4. Small hydrocarbon separation

4.1 C_2H_2–C_2H_4 separation

Separation of acetylene from ethylene is a very important and also challenging industrial separation task. Ethylene obtained from natural gas cracking contains a small amount of acetylene as an impurity, which can serve as a catalyst poison during ethylene polymerization and also lower the quality of the resulting polyethylene. In addition, acetylene can form explosive metal acetylides. It is thus imperative that acetylene in the ethylene product be reduced to an acceptable level. Current main commercial approaches to eliminate acetylene in crude ethylene include partial hydrogenation and solvent extraction. The former process suffers from the need for a noble-metal catalyst and the loss of olefins due to the overhydrogenation to paraffins, while the latter is also disadvantageous in terms of technical and economical aspects because of the low selectivities for acetylene over olefins and the significant loss of solvent after multiple operations. Therefore, it is highly desired to develop a novel alternative C_2H_2–C_2H_4 separation approach.

Our research group realized the first example of the microporous metal–organic frameworks for such challenging separation.[88] **M'MOF-2** and **M'MOF-3** were synthesized *via* solvothermal reaction between the preconstructed metalloligand Cu(SalPyCy), $Zn(NO_3)_2{\cdot}6H_2O$ and H_2BDC or H_2CDC, respectively (Fig. 6a). They are isostructural three-dimensional frameworks in which $Zn_3(COO)_6$ SBUs are bridged by BDC or CDC dianions to from the two-dimensional tessellated sheets that are further pillared by the metalloligand Cu(SalPyCy). The C_2H_2 uptake for desolvated **M'MOFs 2–3a** is systematically higher than C_2H_4 ones (Fig. 6b). Henry's Law selectivity for acetylene/ethylene on **M'MOF-2a** was found to be low (1.6) at 195 K, however, the selectivity jumped to 25.5 for **M'MOF-3a**. Such significantly enhanced separation selectivity of **M'MOF-3a** over **M'MOF-2a** is ascribed to the smaller micropore within **M'MOF-3a** which favors its higher size-exclusion effect.

The promise of the M'MOF strategy to tune micropores promotes us to synthesize four porous isostructural mixed metal–organic frameworks **M'MOF-4–7** in which the pores are systematically modulated by the interplay of both the metalloligands and organic ligands (Fig. 6a).[89] The pure-component sorption isotherm measurements established their foundation for C_2H_2–C_2H_4 separation (Fig. 6b). According to IAST calculations, of these desolvated **M'MOFs 4–7a**, in equilibrium with a 1/99 C_2H_2–C_2H_4 gas mixture at 296 K and a total pressure of 100 kPa, **M'MOF-4a** scores high on both C_2H_2–C_2H_4 adsorption selectivity and C_2H_2 uptake capacity. The separation characteristics were further examined by the transient breakthrough calculations in bed adsorbers packed with **M'MOF-4–7a** with a step input of a 1/99 C_2H_2–C_2H_4 mixture at 296 K and total pressures of 100 kPa. The purity requirement of 40 ppm in the outlet gas can be readily fulfilled by the fixed bed adsorber **M'MOF-4a** under ambient conditions (Fig. 6c). The high C_2H_2–C_2H_4 separation capacity of **M'MOF-4a** was attributed to its high adsorption selectivity and uptake capacity. Analogously, when all **M'MOF-2–7a** are considered, the hierarchy of separation capacities is **M'MOF-3a** > **M'MOF-4a** > **M'MOF-6a** > **M'MOF-2a** > **M'MOF-5a** > **M'MOF-7a** (Fig. 6c).

Adsorptive separation of C_2H_2–C_2H_4 mixtures will be conducted in Pressure Swing Adsorption (PSA) devices whose characteristics are dictated not only by the adsorption selectivity but also by the uptake capacity, as has been emphasized in several recent publications.[1j,90] Fig. 7 presents a plot of the amount of C_2H_4 produced, containing less than 40 ppm of C_2H_2, per L of various chosen adsorbents in a fixed bed, plotted as a function of the adsorption selectivity, S_{ads}.[77] The hierarchy of production capacities is **MgMOF-74** > **CoMOF-74** > **M'MOF-3a** > **M'MOF-4a**. The superior performance of **MgMOF-74** and **CoMOF-74** can be traced to their high capacities to adsorb C_2H_2. **M'MOF-3a**[88] and **M'MOF-4a**[89] have significantly higher selectivities but are subject to capacity limitations.

Herein, we also mention that the first microporous hydrogen-bonded organic framework (HOF) has been developed for

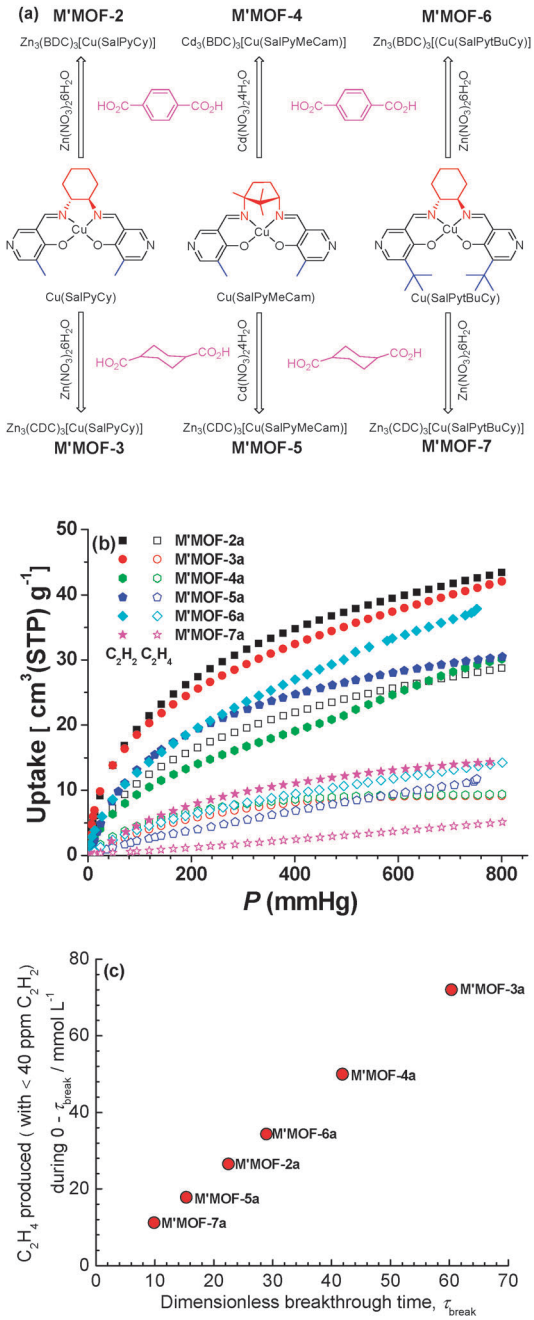

Fig. 6 (a) A schematic diagram for the synthesis of **M'MOF-2-7**. (b) C_2H_2 and C_2H_4 adsorption isotherms for desolvated **M'MOF-2-7a**. (c) A plot of C_2H_4 produced, containing less than 40 ppm of C_2H_2, per L of adsorbents, during the time interval 0–τ_{break}, against the breakthrough time τ_{break} for packed bed adsorbers with a step input of a 1/99 C_2H_2–C_2H_4 mixture at 296 K and total pressures of 100 kPa. The breakthrough time τ_{break} corresponds to the outlet gas containing 40 ppm C_2H_2.

highly selective C_2H_2–C_2H_4 separation at ambient temperature.[91] **HOF-1** is a three-dimensional porous HOF in which each organic building block is connected to four neighboring ones by eight strong hydrogen bonds involving the 2,4-diaminotriazine group. There exist one-dimensional pores along the *c* axis with a size of ~8.2 Å based on the van der Waals radii. One of the amine groups within the 2,4-diaminetriazine

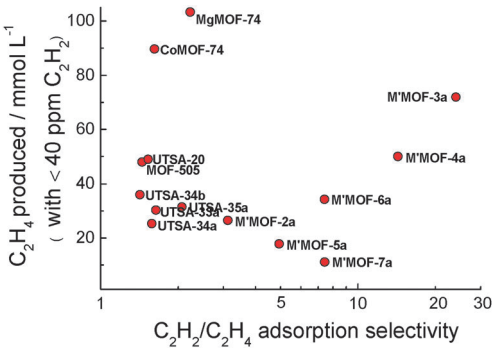

Fig. 7 C_2H_4 produced (of required purity, containing less than 40 ppm of C_2H_2, determined from transient breakthrough simulations) per L of MOFs in fixed bed adsorbers plotted as a function of adsorption selectivity, S_{ads} (calculated from IAST). Reproduced from ref. 77.

moieties is not involved in the hydrogen bonding and thus is exposed on the pore surfaces. The C_2H_2–C_2H_4 molar ratio separation selectivity of 7.6 at 273 K in desolvated **HOF-1a** is significantly higher than those reported in M'MOFs (<3.0). Such high C_2H_2–C_2H_4 separation selectivity can be further increased up to 14.6 at 296 K. The high separation selectivity might be attributed to the narrow pore space within **HOF-1a** and hydrogen bonding interactions of acidic H atoms of the guest acetylene molecules and the basic amine groups of **HOF-1a**.

4.2 C_2–C_1 separation

Separation of C_2 hydrocarbons (C_2s) from methane (C_1) is a very important industrial process. This is because the recovery of C_2 hydrocarbons from methane not only upgrades the quality of natural gas for its efficient usage, but can also provide an alternative chemical source of C_2s for further chemical processing and transformation. Furthermore, C_2s are the main products of oxidative coupling of methane in the process of converting natural gas into a more useful chemical feedstock, thus they certainly need to be separated from the unreacted methane.

Given the fact that these hydrocarbons have the kinetic diameters of 3.3 to 4.4 Å, microporous MOFs with pore sizes comparable to and/or slightly larger than their kinetic diameters will be of special interest as the adsorbents for the separation of these small hydrocarbons. By the framework interpenetration we have targeted the first such microporous MOF **UTSA-36a** [$Zn_2(pba)_2(bdc)$] with pore sizes of 3.1 to 4.8 Å for selective adsorptive separation of C_2H_2, C_2H_4, and C_2H_6 from CH_4.[80] Henry's law separation selectivities are 11 to 25 in the temperature range of 273 to 296 K, which are modest.

To develop microporous MOFs with better C_2–C_1 separation selectivity and capacity, we synthesized two microporous MOFs **UTSA-33a** (Zn_4L) and **UTSA-34b** [$Cu_3(H_2L)$] derived from a novel octacarboxylate linker (L = 1,2,4,5-tetra-(5-isophthalate)benzene).[53,78] Their potentials for separation of C_2 hydrocarbons from methane have been exclusively established by the sorption isotherms and simulated breakthrough experiments. Krishna *et al.*[90] have demonstrated that the dimensionless breakthrough time (see their papers for the definition) is a proper metric for evaluation of different MOFs

in PSA units. This metric combines both the selectivity and capacity factors in an appropriate manner. We compare the breakthrough times of C_2s in outlet gas for equimolar four-component mixtures of C_2H_2, C_2H_4, C_2H_6, and CH_4 in **UTSA-33a** and **UTSA-34b**. It was found that the breakthrough of all C_2s occurs significantly later with **UTSA-34b** (Fig. 8). The longer breakthrough implies that **UTSA-34b** has higher production capacity. Such high separation capacity may be attributed to the high pore volume and/or immobilized open copper sites within **UTSA-34b**. In addition, **UTSA-34b** also exhibits much higher separation selectivity and capacity of C_2H_6 over CH_4 in the equimolar binary mixture of C_2H_6 and CH_4 than the widely investigated **ZIF-8**.[92]

Kitagawa *et al.* investigated CH_4–C_2H_6 separation in flexible two-dimensional porous coordination polymers **CID-5** [Zn(5NO_2-ip)(4,4′-bpy)], **CID-6** [Zn(5MeO-ip)(4,4′-bpy)], and their solid solutions **CID-5/6** [Zn(5NO_2-ip)$_{1-x}$(5MeO-ip)$_x$(4,4′-bpy)] (x = 0.1, 0.2, 0.4).[93] **CID-5** and **CID-6** exhibit different framework flexibility thanks to the different substituent groups of the ligands; **CID-5** is much more flexible than **CID-6**. By changing the ratio of the ligands can the intrinsic flexibility of their solid solutions **CID-5/6** be systematically tuned. **CID-5/6** (x = 0.1) has characteristics similar to those of the pure **CID-5**, whereas **CID-5/6** (x = 0.2, 0.4) are more closely related to the pure **CID-6**. It was found that different framework flexibility led to different kinetic breakthrough curves for a binary CH_4–C_2H_6 gas mixture. **CID-5** and **CID-6** exhibit almost negligible separation, while **CID-5/6** (x = 0.1) can efficiently separate

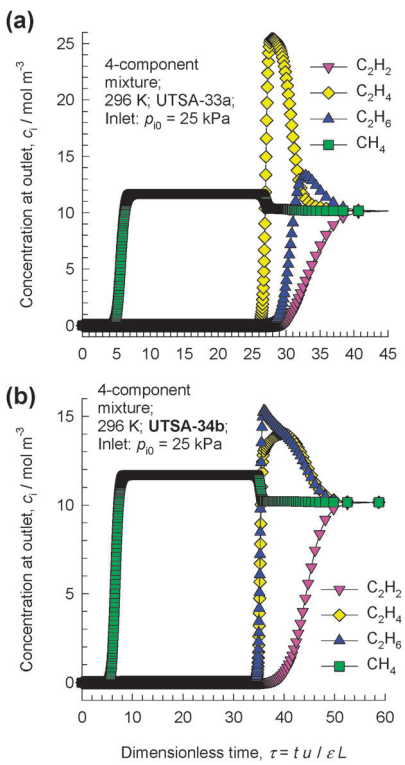

Fig. 8 Transient breakthrough of an equimolar 4-component containing C_2H_2, C_2H_4, C_2H_6 and CH_4 in adsorbers packed with **UTSA-33a** (a) and **UTSA-34b** (b) operating under isothermal conditions at 296 K. The inlet gas is maintained at partial pressures P_{i0} = 25 kPa. Reprinted with permission from ref. 53. Copyright 2011, Wiley.

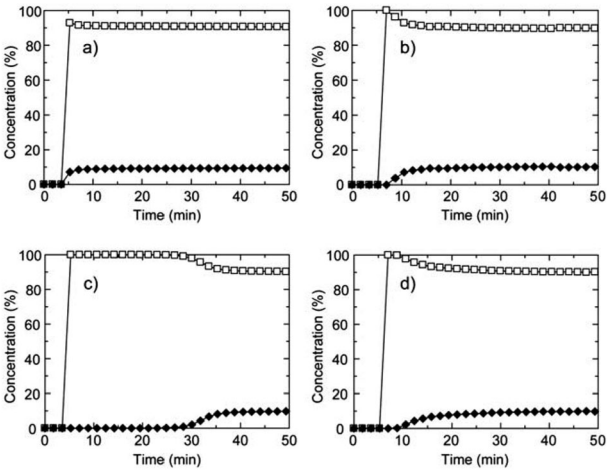

Fig. 9 Breakthrough curves of CH_4–C_2H_6 mixtures (90 : 10, v/v) for (a) **CID-5**, (b) **CID-6**, (c) **CID-5/6** (x = 0.1), and (d) **CID-5/6** (x = 0.4). The open square is CH_4 and the closed diamond is C_2H_6. These are measured at 273 K, the total pressure was 0.80 MPa and the space velocity was 6 min^{-1}. Reproduced from ref. 93.

C_2H_6 from CH_4 (Fig. 9). Thus, the gas separation efficiencies can be optimized by precise tuning of the flexibility in the ligand-based solution compounds.

4.3 Fractionation of light hydrocarbons

Natural gas is one of the most important energy resources that is used worldwide. NG is transported on a gigantic scale both by pipelines and in supertankers. Prior to transportation, NG needs to be conditioned. The conditioning involves dehydration, and removal of acid gases (*e.g.* CO_2, H_2S), and inert gaseous components such as N_2. Hydrocarbons heavier than methane, which are present in NG, such as ethane and propane, have significantly enhanced value as petrochemical feedstocks rather than as components of natural gas used as fuels. The removal of C_2 and C_3 hydrocarbons from NG is traditionally carried out by cryogenic distillation. Adsorptive separation using zeolites (*e.g.* **NaX**, **NaETS-10**), metal–organic frameworks (MOFs), and zeolitic imidazolate frameworks (ZIFs) offers energy-efficient alternatives.

Metal–organic frameworks such as **UTSA-35a** and **UTSA-30a** have been shown to have the capability of separating a mixture of C_1, C_2, and C_3 hydrocarbons into three fractions following the hierarchy of carbon numbers.[79] **MgMOF-74** and **FeMOF-74** offer the more potent capability of fractionating the mixture to yield each individual component in a nearly pure form. This is demonstrated by the pulse chromatographic simulations (Fig. 10).[77] Such a fractionation capability has the potential for considerable energy saving when compared to current technologies that rely on distillation.

4.4 Olefin–paraffin separation

Light olefins, like ethylene and propylene, are important feedstocks in the chemical industry for the production of rubbers, plastics, films and other valuable chemical products. The light olefins are usually obtained by naphtha cracking or dehydrogenation of the corresponding paraffins. In order to obtain the olefin, the separation of the olefins from the uncracked paraffins is required.

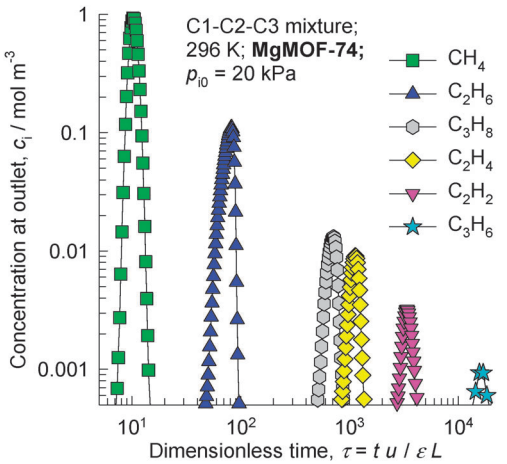

Fig. 10 Pulse chromatographic separation of an equimolar 6-component CH_4–C_2H_2–C_2H_4–C_2H_6–C_3H_6–C_3H_8 mixture with **MgMOF-74** at 296 K. The *x*-axis is the dimensionless time, obtained by dividing the actual time by the characteristic time, $L\varepsilon/u$. Reproduced from ref. 77.

Although traditional cryogenic distillation is a reliable and dominant technology for olefin–paraffin separation, the necessary low temperature and high pressure make it an energy-intensive separation scheme because of their similar sizes and close relative volatilities (the difference in the boiling points of ethylene and ethane is 15 K, and the relative volatility is about 1.2. The difference in the boiling points of propylene and propane is 5.3 K, and the relative volatility is about 1.14). For example, ethylene–ethane separation is carried out at about −25 °C and 320 psig (2.306 MPa) in a column containing over 100 trays, and propylene–propane separation is performed by an equally energy-intensive distillation at about −30 °C and 30 psig (0.308 MPa). It is thus necessary to search for alternatives and more sustainable separation schemes. A number of alternatives have been investigated including extractive distillation, absorption, adsorption and membranes.[94] Among the alternatives considered, adsorption-based separation appears to be one of the promising energy- and cost-effective options. Many commercial adsorbents have been already tested, but the selectivity is not good enough, such as commercial zeolites 4A, 5A and 13X, or adsorbents using π-complexation. Therefore, the development of a suitable sorbent has become a key factor. A few MOFs have been reported to show the potential for olefin–paraffin separation, which is mainly achieved *via* the following three mechanisms: (1) equilibrium based separation; (2) kinetic based separation; and (3) gate-opening effect. Equilibrium separation depends on the differences between relative affinities of the adsorbent towards various adsorbates. Kinetic separation is achieved due to the differences in diffusivities of different molecules. The gate-opening effect is associated with structural transition from a closed nonmicroporous phase to an open porous phase upon gas sorption in which specific threshold pressures control the uptake and release of individual molecules.

4.4.1 Equilibrium based mechanism. For the first time, Bülow and co-workers showed that **HKUST-1** may be used for the separation of ethylene and ethane mixtures.[95] Sorption isotherms for ethylene and ethane on **HKUST-1** at 295 K showed the preferential adsorption of ethylene over ethane especially at low pressure. The selective adsorption was considered to be due to interactions between π-electrons of the double bond in ethylene molecules and partial positive charges of coordinatively unsaturated Cu(II) sites in the framework. This supposition was further supported by the research results from quantum mechanical calculations performed by Nicholson and Bhatia.[96] Their results showed that besides the electrostatic interactions, the hydrogen binding interactions of ethylene with framework oxygen atoms also play an important role in the preferential adsorption. The separation of an ethylene–ethane binary mixture on **HKUST-1** was also evaluated by GCMC simulation.[97] Both computational results suggested a selectivity factor of about 2 for the adsorption of ethylene over ethane at low pressure.

Adsorptive separation of propylene and propane on **HKUST-1** was performed by Chang and co-workers.[98] The pure-component isotherms exhibit that propylene is much more adsorbed than propane in the whole pressure and temperature ranges investigated. Also, the isosteric heats of adsorption for propylene are higher than those for propane in the whole range of adsorption loadings. Similarly, the preferential affinity towards unsaturated propylene gas molecules results from a π-complexation interaction between π orbitals of propylene double bonds with the vacant s-orbitals of the open copper ions, which was supported by UV-Vis spectra of the guest-loaded MOF sample. The separation factors of propylene over propane calculated from the breakthrough curves range from 3.3 (at 313 K) to 5.5 (at 353 K), depending on the operation temperature. The observed selective adsorption and separation properties of **HKUST-1** for propylene and propane are consistent with computational results from molecular simulations.[99] Meanwhile, Rodrigues and co-workers also demonstrated similar performances of **HKUST-1** in the selective adsorption of propylene over propane from both experimental measurements and computational simulations.[100]

The potential of **HKUST-1** for the separation of isobutene and isobutane was checked by Hartmann and co-workers.[101] Adsorption experiments at different temperatures show that a somewhat larger amount of isobutene is adsorbed as compared to isobutane. Nevertheless, the differential enthalpies of adsorption are only different by about 5 kJ mol^{-1}, indicating that a strong interaction between the copper centers and isobutene does not drive the observed difference in adsorption capacity. The simulated breakthrough curves of isobutene and isobutane reveal that a low pressure is favorable for the separation, which has further been confirmed by preliminary breakthrough experiment using an equimolar mixture of isobutane and isobutene with a separation factor of 2.1 at 303 K.

Preferential adsorption of propylene over propane was also observed in a three-dimensional porous framework **FeMIL-100**.[102] Interestingly, the valence of Fe centers generated after activation is dependent on the activation temperature. Only Fe(III) sites are formed upon activation at temperature below 423 K under high vacuum, while reduced Fe(II) sites are generated at higher temperature due to the departure of anionic ligands (F^- and OH^-). It was found that the sorption affinity for propylene over propane is valence-dependent on the Fe centers at low pressures. In the presence of only Fe(III) sites,

similar adsorption enthalpies (-30 kJ mol^{-1}) were observed for propane and propylene. The introduction of Fe(II) sites enhanced the heat of adsorption of propylene at low coverage (-70 kJ mol^{-1}), while that of propane remained almost unchanged. Breakthrough experiments gave a separation factor of 28.9 for propylene over propane on the sample activated at 523 K, and 5.1 for the one activated at 423 K. This result indicates that the presence of Fe(II) site can dramatically improve the separation performance due to its softer metal character.

MgMOF-74 has been suggested by Deng *et al.* as a possible candidate for adsorptive separation of ethylene–ethane and propylene–propane couples on the basis of the single-component adsorption isotherms.[103] Shortly afterwards, Snurr and co-workers systematically investigated the propylene–propane separation in a series of isostructural frameworks **MOF-74-M** (M = Co, Mn, Mg).[104] **CoMOF-74** exhibits the highest thermodynamic propylene–propane selectivity due to strongest π-complexation interaction between the open Co^{2+} sites and the propylene molecules. Most remarkable is that propylene–propane selectivity increases with increasing pressure. The unusual behavior is attributed to the proper match between the size of the propylene molecules and the pore size. When all the metal sites are preferentially occupied by the propylene molecules, only a small amount of pore volume is left and therefore the adsorption of propane is strongly suppressed, thus resulting in a significant increase of the C_3H_6–C_3H_8 selectivity with increasing pressure. This explanation is further supported by the experimental result that the separation selectivities of a smaller C_2H_4–C_2H_6 pair rapidly decrease with increasing pressure. Very recently, Long and co-workers reported that the metal–organic framework **FeMOF-74** exhibited excellent performance for separation of light hydrocarbons.[76] Breakthrough experiments show that this material can separate an equimolar mixture of ethylene and ethane into the pure-component gases of 99% to 99.5% purity. As for an equimolar propylene–propane gas mixture, 100% pure propane and greater than 99% propylene can be obtained. More importantly, breakthrough data obtained for these gas mixtures provide experimental validation of simulations, which in turn predict high selectivities and capacities of this material for the fractionation of 4-component methane–ethane–ethylene–acetylene mixtures, removal of acetylene impurities from ethylene, and membrane based olefin–paraffin separation. The nature of the interaction of these adsorbate molecules within **FeMOF-74** was also studied using neutron powder diffraction. The unsaturated hydrocarbons acetylene, ethylene, and propylene display the *side-on* binding modes with Fe–C distances in the range of 2.42 to 2.60 Å, while the interactions of both ethane and propane with metal cations in **FeMOF-74** are even weaker with the elongated Fe–C distance of ~3 Å.

Selective sorption of olefins over paraffins in two porous ionic crystals $[Cr_3O(OOCCH_2X)_6(H_2O)_3]_4[\alpha\text{-}SiW_{12}O_{40}]$ (X = Cl [Ia], Br [IIa]) was reported by Mizuno and co-workers.[105] They are built up from halogen-substituted macrocations and polyoxometalates (POMs). These two compounds possess analogous one-dimensional winding channels, and the channel walls are composed of oxygen atoms of silicododecatungstates and CH_2X groups of macrocations. Ethylene–ethane and propylene–propane sorption ratios at 298 K and 100 kPa for dehydrated Ib were 3.6 and 6.1, respectively, and the ethylene–ethane sorption ratio at 298 K and 100 kPa for dehydrated IIb was 2.8. The preferential ethylene sorption is ascribed to the electrostatic interaction between the π-electrons of olefins and highly polarized halogen-substituted macrocations and/or polyoxometalates, as demonstrated by ^{13}C MAS NMR and DFT calculation and Monte Carlo simulation.

4.4.2 Kinetic based mechanism. Li and co-workers explored, for the first time, the kinetic separation of propylene and propane performed on three ZIFs, $Zn(2\text{-cim})_2$, $Zn(2\text{-bim})_2$, and **ZIF-8**.[106] Under equilibrium conditions, **ZIF-8** adsorbs essentially the same amount of propylene and propane, and their isosteric heats at low loadings are also similar, indicating that thermodynamic separation of propylene and propane is impractical. However, the single-component diffusion studies reveal that the kinetic separation of propylene and propane by these ZIFs should be highly feasible on the basis of the remarkable differences in their diffusion rates through pore systems. For instance, at 30 °C, the ratios of diffusion rates of propylene and propane through **ZIF-8** and $Zn(2\text{-cim})_2$ are 125 and 60, respectively. The effective size of the pore opening in these MOFs was considered to be the controlling factor determining the separation capability.

Hupp and co-workers reported kinetic separation of propane and propylene in a series of isostructural, noncatenated, zinc-pillared-paddlewheel metal–organic frameworks **DTO**, **TO**, **DBTO** and **BTO**.[107] They are made up of dipyridyl struts and tetracarboxylate struts held together by Zn^{2+} nodes. As shown in Fig. 11, the apertures of top-to-bottom channels can be tuned by 3,6-functionalization of the tetracarboxylate ligands, while the apertures of edge channels can be modulated by functionalization of dipyridine ligands. The kinetic adsorption selectivity for propylene *versus* propane was evaluated from the time-dependent gas uptake profiles. **DBTO** and **BTO** with Br moieties showed much higher kinetic selectivities than those of corresponding **TO** and **DTO** without Br moieties. Considering that the thin rectangular plate morphology of the MOF crystals favors the flow of gas through the top to bottom channels, the large kinetic selectivities observed in **DBTO** and **BTO** were attributed to the reduction in the apertures of top-to-bottom channels, which efficaciously discriminated the two molecules due to their slight difference in size. This explanation was further supported by the decreased kinetic selectivity observed in a ground sample of **DBTO** because of the reduced plane of the top-to-bottom channels.

4.4.3 Gate-opening mechanism. Gascon and co-workers reported the first example of a microporous material **ZIF-7** (Zn_2(bim), bim = benzimidazole) displaying anomalous adsorption selectivity for the alkane in the separation of alkane–alkene mixtures.[108] The sorption isotherms show that alkane and alkene have distinctly different gate-opening pressures. DFT calculations indicate that the difference in the gate-opening pressure is due to stronger adsorption of alkene on the external surface of the **ZIF-7** window entrances. It has been proposed that the reversed alkane selectivity is attributed to a gate-opening effect in which specific opening pressures control the uptake and release of different gas molecules.

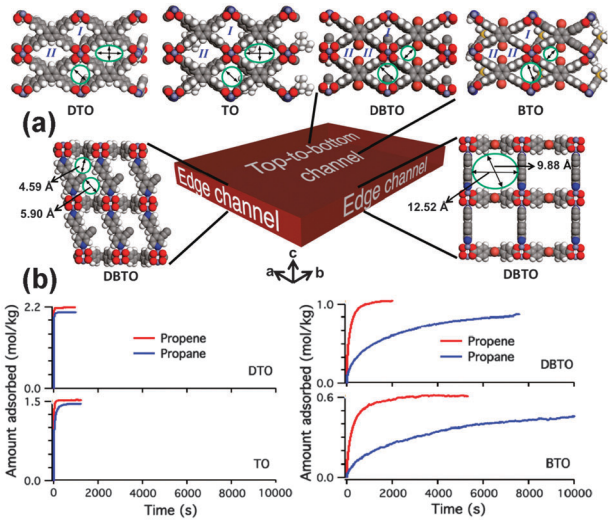

Fig. 11 (a) Crystal packing diagrams of the four isostructural MOFs **DTO**, **TO**, **DBTO**, and **BTO**, showing the pores running along the dipyridyl struts, and crystal packing diagrams of **DBTO** showing the framework pores along the *a* (right) and *b* (left) axes. (b) Time-dependent propylene and propane uptake profiles for **DTO**, **TO**, **DBTO**, and **BTO** MOFs at 30 kPa and 298 K. Reprinted with permission from ref. 107. Copyright 2011, American Chemical Society.

Efficient separation of ethane–ethylene and propane–propylene pairs by **ZIF-7** was further confirmed by breakthrough experiments.

4.4.4 PSA and membrane separation. For olefin–paraffin separation, two different strategies can be adopted: (1) PSA separation in which differences in adsorption strengths are exploited,[94a,109] and (2) membrane separation, relying on differences in diffusion characteristics.[110] Membrane permeation alone cannot produce alkene feedstock of polymer-grade purity, and such separations need to be carried out in hybrid distillation-membrane configurations.[111]

In the adsorption cycle of PSA operations, nearly pure alkane is recovered; the alkene in nearly pure form can be recovered in the desorption cycle by operation with purge gas at higher temperature or lower pressure. In PSA operations, intra-crystalline diffusion limitations are not of prime importance and the transient dynamics of breakthrough in fixed beds can be reasonably well simulated using the methodology developed in recent works.[2j,90] This is also evidenced by the comparisons between experiments and simulations presented in Fig. 12.[76] Thus, breakthrough simulation can be used for screening purpose. Transient breakthrough simulations were carried out to determine the productivity of C_2H_4 produced per L of various chosen MOFs.[77] The results are presented in Fig. 13a as a function of the corresponding adsorption selectivity. The highest productivities are obtained with **FeMOF-74**, **CoMOF-74** and **MgMOF-74**. It is interesting to note that **NaETS-10**[112] has a significantly lower productivity, despite the highest adsorption selectivity. This underscores the fallacy of screening MOFs for separation applications using selectivity as the only metric. This point has been emphasized in the recent literature for CO_2 capture.[2j,113] Fig. 13b presents an

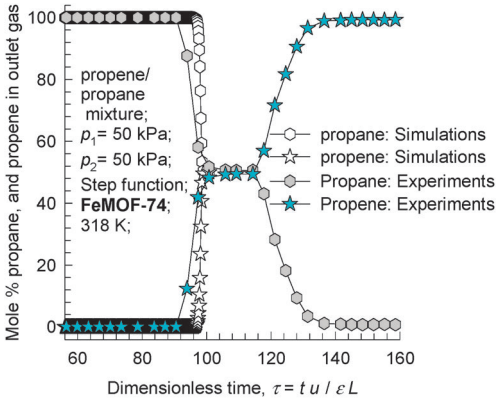

Fig. 12 Comparison of experimentally determined transient breakthrough of an equimolar propylene–propane mixture in an adsorber bed packed with **FeMOF-74** at 318 K and a total pressure of 100 kPa with simulations in which the assumption of the negligible diffusion influence is invoked. Only the adsorption cycle of the simulation is shown here. The *x* axis is the dimensionless time obtained by dividing the actual time by the characteristic contact time, $L\varepsilon/u$.

analogous plot for the productivities of C_3H_6. **FeMOF-74**, **CoMOF-74** and **MgMOF-74** have the best performance. It is interesting to note that **CuBTC (=HKUST-1)** has C_3H_6 productivity comparable to that of **MgMOF-74**, justifying the research on this MOF too.[98a] **FeMIL-100**[102] performs relatively poorly, due to capacity limitations.

Membrane separation of alkene–alkane mixtures is most commonly achieved by choosing pore sizes[107] and window apertures[106,108a,110a,114] in cage-type materials (*e.g.* **CHA**, **DDR**, **ZIF-7**, and **ZIF-8**) to enhance the diffusion selectivities. Small and subtle differences in the bond lengths and bond angles of guest molecules, combined with those of both the window aperture and shape, appear to influence the diffusion selectivities. The window apertures of **ZIF-7** and **ZIF-8** are about 3.2–3.5 Å, and the interactions of the guest molecules and the benzene rings in the windows lead to flexibility and gate opening effects.[108a,115] Li *et al.* have determined the C_3H_6–C_3H_8 diffusion selectivity for **ZIF-8** to be 125.[106] For **ZIF-8** membranes, the C_3H_6–C_3H_8 permeation selectivities are somewhat lower, in the range of 25–40,[110b] because the adsorption selectivity in **ZIF-8** favors the alkane. Analogously, for C_2H_4–C_2H_6 mixtures, the measured permeation selectivity across the **ZIF-8** membrane is in the range of 2–3. These values are lower than the diffusion selectivities because adsorption favors ethane.[110a]

Manufacture of defect-free membranes is a difficult task,[110c] and a lot of current research attention is devoted to the development of mixed matrix membranes in which MOF or ZIF crystals are embedded inside thin polymeric membrane films. Zhang *et al.* reported that C_3H_6–C_3H_8 permeation selectivities are in excess of 100 for a polyimide membrane embedded with **ZIF-8** crystals.[116] If thin defect-free films of **FeMOF-74** or **MgMOF-74** can be mounted onto a membrane support, significantly higher permeabilities can be achieved in comparison to **ZIF-8**, while retaining the high permeation selectivity values. This radical approach has been suggested by Bloch *et al.*,[76] and recent work has shown that **NiMOF-74** membrane films can be made by a seeding technique.[127]

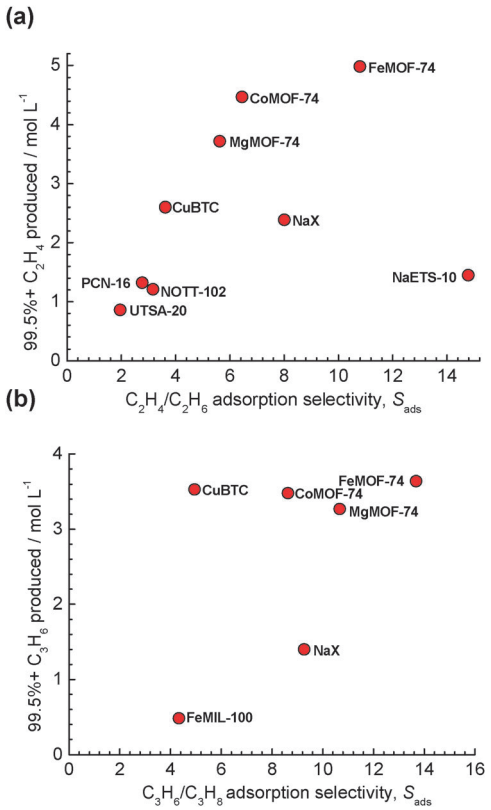

Fig. 13 (a) C_2H_4 produced (of required purity, containing less than 0.5% of C_2H_6, determined from transient breakthrough simulations) per L of MOFs in fixed bed adsorbers plotted as a function of adsorption selectivity, S_{ads} (calculated from IAST). (b) C_3H_6 produced (of required purity, containing less than 0.5% of C_3H_8) per L of MOFs in fixed bed adsorbers plotted as a function of adsorption selectivity, S_{ads}. Note that the data for **FeMOF-74** are obtained at a temperature of 318 K. Reproduced from ref. 77.

4.5 Separation of hexane isomers

Isomerization of alkanes, for the purpose of octane improvement, is a process of importance in the petroleum industry.[117] The product from the isomerization reactor, which commonly uses zeolite MOR as a catalyst, consists of an equilibrium distribution of unreacted *n*-hexane (nhex), along with its mono-branched isomers 2-methylpentane (2mp), 3-methylpentane (3mp) and di-branched isomers 2,2-dimethylbutane (22dmb) and 2,3-dimethylbutane (23dmb). The values of the Research Octane Number (RON) increase with the degree of branching: nhex = 30; 2mp = 74.5; 3mp = 75.5; 22dmb = 94; 23dmb = 105. Therefore di-branched isomers are preferred products in an isomerization process. In current industrial practice, the linear nhex is separated from the branched isomers in an adsorption–separation step that relies on molecular sieving. The adsorbent is **LTA-5A** that consists of cages separated by 4.1 Å sized windows. The windows only allow the diffusion, and adsorption of the linear isomer, and the branched isomers are rejected and removed as products. The unreacted nhex is recycled back to the isomerization reactor. An improved process would require the recycle of both linear and mono-branched isomers to the reactor (Fig. 14). The separation of 22dmb and 23dmb from the remaining isomers is a difficult task because it requires distinguishing molecules based on the degree of branching. There are indications from the patent literatures that this separation can be achieved using a zeolite adsorbent, and a wide variety of zeolites are mentioned as candidate adsorbents.[118] With the wide variety of MOFs being currently available, it is interesting to investigate whether MOFs can be effective for hexane isomer separation required by the ideal process scheme in Fig. 14.

Chen and co-workers reported the first example of microporous MOFs $Zn_2(bdc)_2(dabco)$ for kinetic separation of hexane isomers.[119] There exist two types of intersecting channels of about 7.5 × 7.5 Å along the *a* axis and channels of 3.8 × 4.7 Å along the *b* and *c* axes, respectively. Considering that the kinetic diameters of nhex, 3mp and 22dmb are 4.3, 5.0 and 6.2 Å, respectively, the channels of 3.8 × 4.7 Å can take up the linear nhex but block the branched 3mp and 22dmb, while all these hexane isomers can go through the channel of 7.5 × 7.5 Å. Single-component breakthrough experiments indicate that the adsorption strengths of the hexane isomers decrease as the degree of branching increases. Furthermore, binary and ternary breakthrough experiments have established its potential for kinetic separation of hexane isomers by fixed bed adsorption.

A three-dimensional pillared-layer metal–organic framework $[Zn_2(Hbdc)_2(dmtrz)_2]$ was reported to show the selective adsorption of linear and mono-branched hexane isomers over a di-branched one.[120] There exist one-dimensional channels of 7.0 × 7.0 Å along the *c* axis. Compared to the selective adsorption of nhex over 3mP on $[Zn_2(bdc)_2(dabco)]$, this material shows no obvious selective adsorption between these two isomers. However, it hardly adsorbs 22dmb over the whole pressure range. This might be ascribed to its larger molecule size compared with nhex and 3mp. This indicates it as a potential adsorbent for the separation of nhex and 3mp over 22dmb, which was further confirmed by gas chromatography study.

Adsorption behaviors of hexane isomers were investigated in a rigid zirconium terephthalate **UiO-66**.[121] Multicomponent equimolar breakthrough experiments show that the adsorption hierarchy of structural isomers is opposite to the one observed in conventional adsorbents. Of hexane isomers, branched C_6 isomers are more adsorbed compared to their linear counterparts, 22dmb and 23dmb being the more retained molecules.

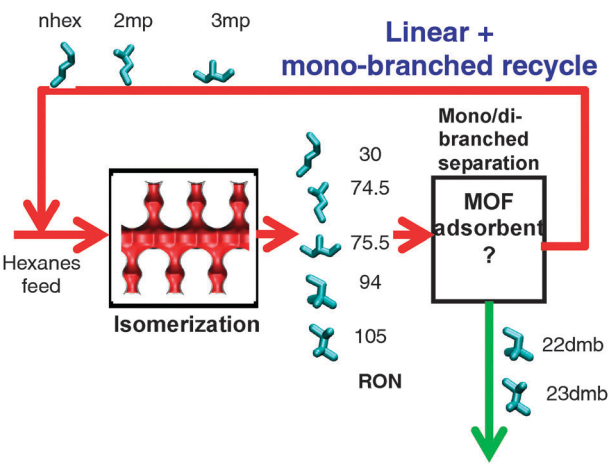

Fig. 14 A suggested improved process for alkane isomerization.

The unusual reversed preferential adsorption of di-branched molecules was considered to be governed by the rotational freedom of the molecules inside the small cavities.

In the study of Bárcia *et al.*, **UiO-66** preferentially adsorbs the dibranched 22dmb and 23dmb molecules, and is also of potential use. In the experiments of Chen *et al.* with $[Zn_2(bdc)_2dabco]$ as an adsorbent, the separation hierarchy of nhex $\gg$ 3mp $\approx$ 22dmb is obtained, which is not the desired one in the process scheme of Fig. 14. A systematic investigation of a wide variety of zeolites and MOFs using molecular simulations for adsorption of 5-component hexane mixtures has revealed that **Co(BDP)**[122] and **MgMOF-74** have the desirable characteristics.[123] Experimental verification of their anticipated performance is yet unavailable.

4.6 Other hydrocarbon separations

Li and co-workers reported the first microporous metal–organic framework $[Cu(hfipbb)(H_2hfipbb)_{0.5}]$ capable of separating normal C_2, C_3 and C_4 olefins and alkanes from all branched and normal hydrocarbons above C_4.[124] The size-exclusion effect is responsible for such unique adsorption properties, which is also supported by gas sorption simulations.

Separation of *cis*-2-butylene, 1-butylene and *trans*-2-butylene was performed in **HKUST-1**.[125] Competitive batch adsorption experiments show that *cis*-2-butylene is preferred the most and the *trans*-2-butylene the least, presumably because the double bond in the *cis*-configuration would be more easily accommodated on the Cu(II) sites within **HKUST-1**. The preference order found for *cis*-2-pentylene, 1-pentylene and *trans*-2-pentylene is also the same as for the butylene isomers. The competitive uptake of *cis*- and *trans*-2-pentylene was further investigated as a function of equilibrium bulk-phase concentration. The separation factors decrease with the increasing concentration.

Separation of C_5-hydrocarbons on three microporous materials **MIL-96**, chabazite, **HKUST-1** was investigated and compared by De Vos and co-workers.[126] **MIL-96** and chabazite preferentially adsorb *trans*-piperylene from a mixture containing all three C_5-diolefin isomers due to a more efficient packing of the *trans* isomer in their pores. Chabazite can separate linear from branched C_5-diolefins, monoolefins and paraffins based on size exclusion of the branched isomers. **MIL-96** can separate diolefins not only from paraffins but also from monoolefins. Preferential uptake of diolefins over alkane or monoolefins is attributed to the entropic effects. **HKUST-1** is able to separate C_5-olefins from paraffins. The preferential adsorption of olefins on **HKUST-1** is due to the interaction of the double bond with the free ligation site on the Cu atoms. Thus, chabazite is suitable for separating all three diolefin isomers. **MIL-96** is capable of separating all three diolefin isomers from C_5-monoolefins and paraffins. Therefore, to fractionalize the C_5-hydrocarbon cut into individual stream, the combined use of MOFs and zeolites may be needed.

5. Conclusion

Microporous metal–organic frameworks differentiate themselves from other traditional porous materials such as zeolite and carbon materials because of their high porosities, tunable pore structures and immobilized functional sites on the pore surfaces. These unique features have enabled microporous MOFs as very promising and practically useful materials for the storage and separation of hydrocarbons. It is envisioned that the extensive research on this very important topic will not only lead to some novel discoveries, but will also facilitate the implementation of some porous MOFs for their daily and industrial usage for hydrocarbon storage and separation in the near future.

Abbreviations

pzdc	pyrazine-2,3-dicarboxylate
pyz	pyrazine
bdc	benzene-1,4-dicarboxylate
1,4-ndc	naphthalene-1,4-dicarboxylate
2,6-ndc	naphthalene-2,6-dicarboxylate
2,7-ndc	naphthalene-2,7-dicarboxylate
adc	anthracene-9,10-dicarboxylate
dabco	1,4-diazabicyclo[2.2.2]octane
Hetz	3,5-diethyl-1,2,4-triazole
dhtp	2,5-dihydroxyterephthalate
dobdc	2,5-dioxidobenzene-1,4-dicarboxylate
H_2bpz	3,3′,5,5′-tetramethyl-4,4′-bipyrazole
Hbta	1,2,3-benzenetriazole
H_2tda	thiophene-2,5-dicarboxylic acid
1,2,4-btc	benzene-1,2,4-tricarboxylate
H_2bdc-OH	2-hydroxybenzene-1,4-dicarboxylic acid
4,4′-bpy	4,4′-bipyridine
Hpba	4-(4-pyridyl)benzoic acid
ebtc	1,1′-ethynebenzene-3,3′5,5′-tetracarboxylate
bpt	biphenyl-3,4′,5-tricarboxylate
azpy	4,4′-azopyridine
pia	*N*-(pyridin-4-yl)isonicotinamide
fma	fumarate
sdc	styrenedicarboxylate
bpdc	biphenyl-4,4′-dicarboxylate
ted	triethylenediamine
adip	5,5′-(9,10-anthracenediyl)diisophthalate
H_6bhb	3,3′,3″,5,5′,5″-benzene-1,3,5-triyl-hexabenzoic acid
H_2bpydb	4,4′-(4,4′-bipyridine-2,6-diyl)dibenzoic acid
btb	benzene-1,3,5-tribenzoate
Hpba	4-(4-pyridyl) benzoic acid
5NO_2-ip	5-nitroisophthalate
5MeO-ip	5-methoxyisophthalate
2-cim	2-chloroimidazolate
2-bim	2-bromoimidazolate
2-meim	2-methylimidazolate
bim	benzimidazole
H_2hfipbb	4,4′-(hexafluoroisopropylidene)bis(benzoic acid)
nhex	*n*-hexane
3mp	3-methylpentane
22dmb	2,2-dimethylbutane
Hdmtrz	3,5-dimethyl-1H,1,2,4-triazole
tptc	[1,1′:3′,1″-terphenyl]-4,4″,5′-tricarboxylate
tdpat	2,4,6-tris(3,5-dicarboxylphenylamino)-1,3,5-triazine
H_2BDP	1,4-benzenedi(4′-pyrazolyl)
bcu	body centered cubic
RON	research octane number

Acknowledgements

This work was supported by an AX-1730 from Welch Foundation (BC).

Notes and references

1 (*a*) O. M. Yaghi, M. O'Keeffe, N. W. Ockwig, H. K. Chae, M. Eddaoudi and J. Kim, *Nature*, 2003, **423**, 705–714; (*b*) M. O'Keeffe and O. M. Yaghi, *Chem. Rev.*, 2012, **112**, 675–702; (*c*) S. Kitagawa, R. Kitaura and S.-i. Noro, *Angew. Chem., Int. Ed.*, 2004, **43**, 2334–2375; (*d*) S. Horike, S. Shimomura and S. Kitagawa, *Nat. Chem.*, 2009, **1**, 695–704; (*e*) G. Férey and C. Serre, *Chem. Soc. Rev.*, 2009, **38**, 1380–1399; (*f*) I. Imaz, M. R.-M. Nez, J. An, I. S. Font, N. L. Rosi and D. Maspoch, *Chem. Commun.*, 2011, **47**, 7287–7302; (*g*) G. K. H. Shimizu, R. Vaidhyanathan and J. M. Taylor, *Chem. Soc. Rev.*, 2009, **38**, 1430–1449; (*h*) S. M. Cohen, *Chem. Rev.*, 2012, **112**, 970–1000; (*i*) C. Wang, T. Zhang and W. Lin, *Chem. Rev.*, 2012, **112**, 1084–1104; (*j*) J.-P. Zhang, Y.-B. Zhang, J.-B. Lin and X.-M. Chen, *Chem. Rev.*, 2012, **112**, 1001–1033; (*k*) H.-L. Jiang and Q. Xu, *Chem. Commun.*, 2011, **47**, 3351–3370; (*l*) C. Zou and C.-D. Wu, *Dalton Trans.*, 2012, **41**, 3879–3888; (*m*) W. Xuan, C. Zhu, Y. Liu and Y. Cui, *Chem. Soc. Rev.*, 2012, **41**, 1677–1695; (*n*) B. Chen, S. Xiang and G. Qian, *Acc. Chem. Res.*, 2010, **43**, 1115–1124.

2 (*a*) R. Vaidhyanathan, S. S. Iremonger, G. K. H. Shimizu, P. G. Boyd, S. Alavi and T. K. Woo, *Science*, 2010, **330**, 650–653; (*b*) J. An, S. J. Geib and N. L. Rosi, *J. Am. Chem. Soc.*, 2010, **132**, 38–39; (*c*) E. Q. Procopio, F. Linares, C. Montoro, V. Colombo, A. Maspero, E. Barea and J. A. R. Navarro, *Angew. Chem., Int. Ed.*, 2010, **49**, 7308–7311; (*d*) T. Panda, P. Pachfule, Y. Chen, J. Jiang and R. Banerjee, *Chem. Commun.*, 2011, **47**, 2011–2013; (*e*) H.-L. Jiang, Y. Tatsu, Z.-H. Lu and Q. Xu, *J. Am. Chem. Soc.*, 2010, **132**, 5586–5587; (*f*) Q. Lin, T. Wu, S.-T. Zheng, X. Bu and P. Feng, *J. Am. Chem. Soc.*, 2012, **134**, 784–787; (*g*) J.-P. Zhang and X.-M. Chen, *J. Am. Chem. Soc.*, 2009, **131**, 5516–5521; (*h*) H. Wu, W. Zhou and T. Yildirim, *J. Am. Chem. Soc.*, 2009, **131**, 4995–5000; (*i*) Y.-X. Tan, Y.-P. He and J. Zhang, *Chem. Commun.*, 2011, **47**, 10647–10649; (*j*) S. Xiang, Y. He, Z. Zhang, H. Wu, W. Zhou, R. Krishna and B. Chen, *Nat. Commun.*, 2012, **3**, 954; (*k*) M. C. Das, S. Xiang, Z. Zhang and B. Chen, *Angew. Chem., Int. Ed.*, 2011, **50**, 10510–10520.

3 (*a*) L. J. Murray, M. Dincă and J. R. Long, *Chem. Soc. Rev.*, 2009, **38**, 1294–1314; (*b*) M. P. Suh, H. J. Park, T. K. Prasad and D.-W. Lim, *Chem. Rev.*, 2012, **112**, 782–835; (*c*) R. B. Getman, Y.-S. Bae, C. E. Wilmer and R. Q. Snurr, *Chem. Rev.*, 2012, **112**, 703–723.

4 (*a*) J.-R. Li, J. Sculley and H.-C. Zhou, *Chem. Rev.*, 2012, **112**, 869–932; (*b*) H. Wu, Q. Gong, D. H. Olson and J. Li, *Chem. Rev.*, 2012, **112**, 836–868; (*c*) K. Sumida, D. L. Rogow, J. A. Mason, T. M. McDonald, E. D. Bloch, Z. R. Herm, T.-H. Bae and J. R. Long, *Chem. Rev.*, 2012, **112**, 724–781; (*d*) Y.-S. Bae and R. Q. Snurr, *Angew. Chem., Int. Ed.*, 2011, **50**, 11586–11596; (*e*) Z. Zhang, S. Xiang and B. Chen, *CrystEngComm*, 2011, **13**, 5983–5992; (*f*) Y. Liu, W. Xuan and Y. Cui, *Adv. Mater.*, 2010, **22**, 4112–4135; (*g*) Z.-Y. Gu, C.-X. Yang, N. Chang and X.-P. Yan, *Acc. Chem. Res.*, 2012, **45**, 734–745.

5 (*a*) L. Ma, C. Abney and W. Lin, *Chem. Soc. Rev.*, 2009, **38**, 1248–1256; (*b*) J. Lee, O. K. Farha, J. Roberts, K. A. Scheidt, S. T. Nguyen and J. T. Hupp, *Chem. Soc. Rev.*, 2009, **38**, 1450–1459; (*c*) D. Farrusseng, S. Aguado and C. Pinel, *Angew. Chem., Int. Ed.*, 2009, **48**, 7502–7513; (*d*) A. Corma, H. García and F. X. L. i. Xamena, *Chem. Rev.*, 2010, **110**, 4606–4655; (*e*) G. Nickerl, A. Henschel, R. Grünker, K. Gedrich and S. Kaskel, *Chem. Eng. Technol.*, 2011, **83**, 90–103; (*f*) M. Yoon, R. Srirambalaji and K. Kim, *Chem. Rev.*, 2012, **112**, 1196–1231.

6 (*a*) L. E. Kreno, K. Leong, O. K. Farha, M. Allendorf, R. P. V. Duyne and J. T. Hupp, *Chem. Rev.*, 2012, **112**, 1105–1125; (*b*) Y. Cui, Y. Yue, G. Qian and B. Chen, *Chem. Rev.*, 2012, **112**, 1126–1162.

7 (*a*) A. C. McKinlay, R. E. Morris, P. Horcajada, G. Férey, R. Gref, P. Couvreur and C. Serre, *Angew. Chem., Int. Ed.*, 2010, **49**, 6260–6266; (*b*) P. Horcajada, T. Chalati, C. Serre, B. Gillet, C. Sebrie, T. Baati, J. F. Eubank, D. Heurtaux, P. Clayette, C. Kreuz, J.-S. Chang, Y. K. Hwang, V. Marsaud, P.-N. Bories, L. Cynober, S. Gil, G. Férey, P. Couvreur and R. Gref, *Nat. Mater.*, 2010, **9**, 172–178; (*c*) P. Horcajada, R. Gref, T. Baati, P. K. Allan, G. Maurin, P. Couvreur, G. Férey, R. E. Morris and C. Serre, *Chem. Rev.*, 2012, **112**, 1232–1268.

8 (*a*) N. C. Jeong, B. Samanta, C. Y. Lee, O. K. Farha and J. T. Hupp, *J. Am. Chem. Soc.*, 2012, **134**, 51–54; (*b*) E. Pardo, C. Train, G. Gontard, K. Boubekeur, O. Fabelo, H. Liu, B. Dkhil, F. Lloret, K. Nakagawa, H. Tokoro, S.-i. Ohkoshi and M. Verdaguer, *J. Am. Chem. Soc.*, 2011, **133**, 15328–15331; (*c*) S. C. Sahoo, T. Kundu and R. Banerjee, *J. Am. Chem. Soc.*, 2011, **133**, 17950–17958; (*d*) J. A. Hurd, R. Vaidhyanathan, V. Thangadurai, C. I. Ratcliffe, I. L. Moudrakovski and G. K. H. Shimizu, *Nat. Chem.*, 2009, **1**, 705–710; (*e*) M. Sadakiyo, T. Yamada and H. Kitagawa, *J. Am. Chem. Soc.*, 2009, **131**, 9906–9907.

9 (*a*) M. Yaghi and H. Li, *J. Am. Chem. Soc.*, 1995, **117**, 10401–10402; (*b*) O. M. Yaghi, G. Li and H. Li, *Nature*, 1995, **378**, 703–706.

10 H. Li, M. Eddaoudi, M. O'Keeffe and O. M. Yaghi, *Nature*, 1999, **402**, 276–279.

11 S. R. Batten, N. R. Champness, X.-M. Chen, J. Garcia-Martinez, S. Kitagawa, L. Öhrström, M. O'Keeffe, M. P. Suhh and J. Reedijk, *CrystEngComm*, 2012, **14**, 3001–3004.

12 (*a*) R. J. Kuppler, D. J. Timmons, Q.-R. Fang, J.-R. Li, T. A. Makal, M. D. Young, D. Yuan, D. Zhao, W. Zhuang and H.-C. Zhou, *Coord. Chem. Rev.*, 2009, **253**, 3042–3066; (*b*) S. Ma, *Pure Appl. Chem.*, 2009, **81**, 2235–2251; (*c*) S. Ma and H.-C. Zhou, *Chem. Commun.*, 2010, **46**, 44–53; (*d*) X. Lin, N. R. Champness and M. Schröder, *Top. Curr. Chem.*, 2010, **293**, 35–76; (*e*) W. Zhou, *Chem. Rec.*, 2010, **10**, 200–204; (*f*) K. Konstas, T. Osl, Y. Yang, M. Batten, N. Burke, A. J. Hill and M. R. Hilla, *J. Mater. Chem.*, 2012, **22**, 16698–16708.

13 T. Burchell and M. Rogers, *SAE Tech. Pap. Ser.*, 2000, 2000-01-2205.

14 D. Lozano-Castelló, J. Alcañiz-Monge, M. A. d. l. Casa-Lillo, D. Cazorla-Amorós and A. Linares-Solano, *Fuel*, 2002, **81**, 1777–1803.

15 M. Kondo, T. Yoshitomi, K. Seki, H. Matsuzaka and S. Kitagawa, *Angew. Chem., Int. Ed. Engl.*, 1997, **36**, 1725–1727.

16 M. Kondo, M. Shimamura, S.-i. Noro, S. Minakoshi, A. Asami, K. Seki and S. Kitagawa, *Chem. Mater.*, 2000, **12**, 1288–1299.

17 M. Kondo, T. Okubo, A. Asami, S.-i. Noro, T. Yoshitomi, S. Kitagawa, T. Ishii, H. Matsuzaka and K. Seki, *Angew. Chem., Int. Ed.*, 1999, **38**, 140–143.

18 (*a*) S.-i. Noro, S. Kitagawa, M. Kondo and K. Seki, *Angew. Chem., Int. Ed.*, 2000, **39**, 2082–2084; (*b*) S.-i. Noro, R. Kitaura, M. Kondo, S. Kitagawa, T. Ishii, H. Matsuzaka and M. Yamashita, *J. Am. Chem. Soc.*, 2002, **124**, 2568–2583.

19 (*a*) K. Seki, *Chem. Commun.*, 2001, 1496–1497; (*b*) K. Seki, S. Takamizawa and W. Mori, *Chem. Lett.*, 2001, 332–333; (*c*) K. Seki and W. Mori, *J. Phys. Chem. B*, 2002, **106**, 1380–1385.

20 K. Seki, *Phys. Chem. Chem. Phys.*, 2002, **4**, 1968–1971.

21 D. F. Quinn and J. A. MacDonald, *Carbon*, 1992, **30**, 1097–1103.

22 (*a*) H. Kim, D. G. Samsonenko, S. Das, G.-H. Kim, H.-S. Lee, D. N. Dybtsev, E. A. Berdonosova and K. Kim, *Chem.–Asian J.*, 2009, **4**, 886–891; (*b*) I. Senkovska and S. Kaskel, *Microporous Mesoporous Mater.*, 2008, **112**, 108–115.

23 (*a*) H. Wang, J. Getzschmann, I. Senkovska and S. Kaskel, *Microporous Mesoporous Mater.*, 2008, **116**, 653–657; (*b*) L.-G. Zhua and H.-P. Xiao, *Z. Anorg. Allg. Chem.*, 2008, **634**, 845–847.

24 M. Eddaoudi, J. Kim, N. Rosi, D. Vodak, J. Wachter, M. O'Keeffe and O. M. Yaghi, *Science*, 2002, **295**, 469–472.

25 T. Düren, L. Sarkisov, O. M. Yaghi and R. Q. Snurr, *Langmuir*, 2004, **20**, 2683–2689.

26 S. Ma, X.-S. Wang, C. D. Collier, E. S. Manis and H.-C. Zhou, *Inorg. Chem.*, 2007, **46**, 8499–8501.

27 X.-S. Wang, S. Ma, K. Rauch, J. M. Simmons, D. Yuan, X. Wang, T. Yildirim, W. C. Cole, J. J. López, A. d. Meijere and H.-C. Zhou, *Chem. Mater.*, 2008, **20**, 3145–3152.

28 S. Ma, D. Sun, J. M. Simmons, C. D. Collier, D. Yuan and H.-C. Zhou, *J. Am. Chem. Soc.*, 2008, **130**, 1012–1016.

29 D. Sun, S. Ma, J. M. Simmons, J.-R. Li, D. Yuan and H.-C. Zhou, *Chem. Commun.*, 2010, **46**, 1329–1331.

30 D. Zhao, D. Yuan, A. Yakovenko and H.-C. Zhou, *Chem. Commun.*, 2010, **46**, 4196–4198.
31 C. E. Wilmer, M. Leaf, C. Y. Lee, O. K. Farha, B. G. Hauser, J. T. Hupp and R. Q. Snurr, *Nat. Chem.*, 2012, **4**, 83–89.
32 D. Yuan, D. Zhao, D. Sun and H.-C. Zhou, *Angew. Chem., Int. Ed.*, 2010, **49**, 5357–5361.
33 Y. Yan, S. Yang, A. J. Blake, W. Lewis, E. Poirier, S. A. Barnett, N. R. Champness and M. Schröder, *Chem. Commun.*, 2011, **47**, 9995–9997.
34 M. Tagliabue, C. Rizzo, R. Millini, P. D. C. Dietzel, R. Blom and S. Zanardi, *J. Porous Mater.*, 2011, **18**, 289–296.
35 Z. Guo, H. Wu, G. Srinivas, Y. Zhou, S. Xiang, Z. Chen, Y. Yang, W. Zhou, M. O'Keeffe and B. Chen, *Angew. Chem., Int. Ed.*, 2011, **50**, 3178–3181.
36 (*a*) Y. Kubota, M. Takata, R. Kitaura, R. Matsuda, T. C. Kobayashi and S. Kitagawa, *J. Nanosci. Nanotechnol.*, 2009, **9**, 69–76; (*b*) J. Getzschmann, I. Senkovska, D. Wallacher, M. Tovar, D. Fairen-Jimenez, T. Düren, J. M. van Baten, R. Krishna and S. Kaskel, *Microporous Mesoporous Mater.*, 2010, **136**, 50–58.
37 H. Wu, J. M. Simmons, Y. Liu, C. M. Brown, X.-S. Wang, S. Ma, V. K. Peterson, P. D. Southon, C. J. Kepert, H.-C. Zhou, T. Yildirim and W. Zhou, *Chem.–Eur. J.*, 2010, **16**, 5205–5214.
38 D. Y. Siberio-Pérez, A. G. Wong-Foy, O. M. Yaghi and A. J. Matzger, *Chem. Mater.*, 2007, **19**, 3681–3685.
39 R. Kitaura, K. Seki, G. Akiyama and S. Kitagawa, *Angew. Chem., Int. Ed.*, 2003, **42**, 428–431.
40 K. Seki, S. Takamizawa and W. Mori, *Chem. Lett.*, 2001, 122–123.
41 W. Lu, D. Yuan, T. A. Makal, J.-R. Li and H.-C. Zhou, *Angew. Chem., Int. Ed.*, 2012, **51**, 1580–1584.
42 C. Tan, S. Yang, N. R. Champness, X. Lin, A. J. Blake, W. Lewis and M. Schröder, *Chem. Commun.*, 2011, **47**, 4487–4489.
43 I. Senkovska, F. Hoffmann, M. Fröba, J. Getzschmann, W. Böhlmann and S. Kaskel, *Microporous Mesoporous Mater.*, 2009, **122**, 93–98.
44 N. Klein, I. Senkovska, K. Gedrich, U. Stoeck, A. Henschel, U. Mueller and S. Kaskel, *Angew. Chem., Int. Ed.*, 2009, **48**, 9954–9957.
45 N. Klein, H. C. Hoffmann, A. Cadiau, J. Getzschmann, M. R. Lohe, S. Paasch, T. Heydenreich, K. Adil, I. Senkovska, E. Brunner and S. Kaskel, *J. Mater. Chem.*, 2012, **22**, 10303–10312.
46 K. Gedrich, I. Senkovska, N. Klein, U. Stoeck, A. Henschel, M. R. Lohe, I. A. Baburin, U. Mueller and S. Kaskel, *Angew. Chem., Int. Ed.*, 2010, **49**, 8489–8492.
47 R. Grünker, I. Senkovska, R. Biedermann, N. Klein, M. R. Lohe, P. Müller and S. Kaskel, *Chem. Commun.*, 2011, **47**, 490–492.
48 N. Klein, I. Senkovska, I. A. Baburin, R. Grünker, U. Stoeck, M. Schlichtenmayer, B. Streppel, U. Mueller, S. Leoni, M. Hirscher and S. Kaskel, *Chem.–Eur. J.*, 2011, **17**, 13007–13016.
49 H. Furukawa, N. Ko, Y. B. Go, N. Aratani, S. B. Choi, E. Choi, A. Ö. Yazaydin, R. Q. Snurr, M. O'Keeffe, J. Kim and O. M. Yaghi, *Science*, 2010, **329**, 424–428.
50 (*a*) F. Millange, C. Serre and G. Férey, *Chem. Commun.*, 2002, 822–823; (*b*) S. Bourrelly, P. L. Llewellyn, C. Serre, F. Millange, T. Loiseau and G. Férey, *J. Am. Chem. Soc.*, 2005, **127**, 13519–13521.
51 P. Rallapalli, D. Patil, K. P. Prasanth, R. S. Somani, R. V. Jasra and H. C. Bajaj, *J. Porous Mater.*, 2010, **17**, 523–528.
52 P. L. Llewellyn, S. Bourrelly, C. Serre, A. Vimont, M. Daturi, L. Hamon, G. D. Weireld, J.-S. Chang, D.-Y. Hong, Y. K. Hwang, S. H. Jhung and G. Férey, *Langmuir*, 2008, **24**, 7245–7250.
53 Y. He, Z. Zhang, S. Xiang, H. Wu, F. R. Fronczek, W. Zhou, R. Krishna, M. O'Keeffe and B. Chen, *Chem.–Eur. J.*, 2012, **18**, 1901–1904.
54 M. C. Das, H. Xu, Z. Wang, G. Srinivas, W. Zhou, Y.-F. Yue, V. N. Nesterov, G. Qian and B. Chen, *Chem. Commun.*, 2011, **47**, 11715–11717.
55 H. J. Park, Y. E. Cheon and M. P. Suh, *Chem.–Eur. J.*, 2010, **16**, 11662–11669.
56 T. K. Prasad, D. H. Hong and M. P. Suh, *Chem.–Eur. J.*, 2010, **16**, 14043–14050.
57 T. K. Prasad and M. P. Suh, *Chem.–Eur. J.*, 2012, **18**, 8673–8680.
58 H. J. Park, D.-W. Lim, W. S. Yang, T.-R. Oh and M. P. Suh, *Chem.–Eur. J.*, 2011, **17**, 7251–7260.
59 W. Zhou, H. Wu, M. R. Hartman and T. Yildirim, *J. Phys. Chem. C*, 2007, **111**, 16131–16137.
60 M. K. Sharma, I. Senkovska, S. Kaskel and P. K. Bharadwaj, *Inorg. Chem.*, 2011, **50**, 539–544.
61 M. Xue, Y. Liu, R. M. Schaffino, S. Xiang, X. Zhao, G.-S. Zhu, S.-L. Qiu and B. Chen, *Inorg. Chem.*, 2009, **48**, 4649–4651.
62 M. Park, D. Moon, J. W. Yoon, J.-S. Chang and M. S. Lah, *Chem. Commun.*, 2009, 2026–2028.
63 J. Y. Lee, L. Pan, X. Huang, T. J. Emge and J. Li, *Adv. Funct. Mater.*, 2011, **21**, 993–998.
64 D. Han, F.-L. Jiang, M.-Y. Wu, L. Chen, Q.-H. Chen and M.-C. Hong, *Chem. Commun.*, 2011, **47**, 9861–9863.
65 D. Liu, H. Wu, S. Wang, Z. Xie, J. Li and W. Lin, *Chem. Sci.*, 2012, **3**, 3032–3037.
66 C. Hou, Q. Liu, J. Fan, Y. Zhao, P. Wang and W.-Y. Sun, *Inorg. Chem.*, 2012, **51**, 8402–8408.
67 B. Li, Z. Zhang, Y. Li, K. Yao, Y. Zhu, Z. Deng, F. Yang, X. Zhou, G. Li, H. Wu, N. Nijem, Y. J. Chabal, Z. Lai, Y. Han, Z. Shi, S. Feng and J. Li, *Angew. Chem., Int. Ed.*, 2012, **51**, 1412–1415.
68 R. Matsuda, R. Kitaura, S. Kitagawa, Y. Kubota, R. V. Belosludov, T. C. Kobayashi, H. Sakamoto, T. Chiba, M. Takata, Y. Kawazoe and Y. Mita, *Nature*, 2005, **436**, 238–241.
69 D. Tanaka, M. Higuchi, S. Horike, R. Matsuda, Y. Kinoshita, N. Yanai and S. Kitagawa, *Chem.–Asian J.*, 2008, **3**, 1343–1349.
70 D. G. Samsonenko, H. Kim, Y. Sun, G.-H. Kim, H.-S. Lee and K. Kim, *Chem.–Asian J.*, 2007, **2**, 484–488.
71 S. Xiang, W. Zhou, J. M. Gallegos, Y. Liu and B. Chen, *J. Am. Chem. Soc.*, 2009, **131**, 12415–12419.
72 B. Chen, C. Liang, J. Yang, D. S. Contreras, Y. L. Clancy, E. B. Lobkovsky, O. M. Yaghi and S. Dai, *Angew. Chem., Int. Ed.*, 2006, **45**, 1390–1393.
73 S. Xiang, W. Zhou, Z. Zhang, M. A. Green, Y. Liu and B. Chen, *Angew. Chem., Int. Ed.*, 2010, **49**, 4615–4618.
74 S. M. Chavan, G. C. Shearer, E. Bloch and S. Bordiga, *ChemPhysChem*, 2012, **13**, 445–448.
75 J.-P. Zhang and S. Kitagawa, *J. Am. Chem. Soc.*, 2008, **130**, 907–917.
76 E. D. Bloch, W. L. Queen, R. Krishna, J. M. Zadrozny, C. M. Brown and J. R. Long, *Science*, 2012, **335**, 1606–1610.
77 Y. He, R. Krishna and B. Chen, *Energy Environ. Sci.*, 2012, **5**, 9107–9120.
78 Y. He, Z. Zhang, S. Xiang, F. R. Fronczek, R. Krishna and B. Chen, *Chem.–Eur. J.*, 2012, **18**, 613–619.
79 (*a*) Y. He, Z. Zhang, S. Xiang, F. R. Fronczek, R. Krishna and B. Chen, *Chem. Commun.*, 2012, **48**, 6493–6495; (*b*) Y. He, S. Xiang, Z. Zhang, S. Xiong, F. R. Fronczek, R. Krishna, M. O'Keeffee and B. Chen, *Chem. Commun.*, 2012, **48**, 10856–10858.
80 M. C. Das, H. Xu, S. Xiang, Z. Zhang, H. D. Arman, G. Qian and B. Chen, *Chem.–Eur. J.*, 2011, **17**, 7817–7822.
81 Y. Hu, S. Xiang, W. Zhang, Z. Zhang, L. Wang, J. Bai and B. Chen, *Chem. Commun.*, 2009, 7551–7553.
82 Z. Zhang, S. Xiang, Y.-S. Chen, S. M. Lee, T. Phely-Bobin and B. Chen, *Inorg. Chem.*, 2010, **49**, 8444–8448.
83 Z. Zhang, S. Xiang, X. Rao, Q. Zheng, F. R. Fronczek, G. Qian and B. Chen, *Chem. Commun.*, 2010, **46**, 7205–7207.
84 Z. Chen, S. Xiang, H. D. Arman, J. U. Mondal, P. Li, D. Zhao and B. Chen, *Inorg. Chem.*, 2011, **50**, 3442–3446.
85 Z. Chen, S. Xiang, H. D. Arman, P. Li, S. Tidrow, D. Zhao and B. Chen, *Eur. J. Inorg. Chem.*, 2010, 3745–3749.
86 Y.-S. Xue, Y. He, S.-B. Ren, Y. Yue, L. Zhou, Y.-Z. Li, H.-B. Du, X.-Z. You and B. Chen, *J. Mater. Chem.*, 2012, **22**, 10195–10199.
87 Z. Guo, H. Xu, S. Su, J. Cai, S. Dang, S. Xiang, G. Qian, H. Zhang, M. O'Keeffe and B. Chen, *Chem. Commun.*, 2011, **47**, 5551–5553.
88 S. Xiang, Z. Zhang, C.-G. Zhao, K. Hong, X. Zhao, D.-L. Ding, M.-H. Xie, C.-D. Wu, R. Gill, K. M. Thomas and B. Chen, *Nat. Commun.*, 2010, **2**, 204.
89 M. C. Das, Q. Guo, Y. He, J. Kim, C.-G. Zhao, K. Hong, S. Xiang, Z. Zhang, K. M. Thomas, R. Krishna and B. Chen, *J. Am. Chem. Soc.*, 2012, **134**, 8703–8710.

90 R. Krishna and J. R. Long, *J. Phys. Chem. C*, 2011, **115**, 12941–12950.
91 Y. He, S. Xiang and B. Chen, *J. Am. Chem. Soc.*, 2011, **133**, 14570–14573.
92 S. C. Reyes, J. G. Santiesteban, Z. Ni, C. S. Paur, P. Kortunov, J. Zengel and H. W. Deckman, *U.S Pat*, 2009, US2009/0216059A1.
93 S. Horike, Y. Inubushi, T. Hori, T. Fukushima and S. Kitagawa, *Chem. Sci.*, 2012, **3**, 116–120.
94 (*a*) R. B. Eldridge, *Ind. Eng. Chem. Res.*, 1993, **32**, 2208–2212; (*b*) R. Faiz and K. Li, *Chem. Eng. Sci.*, 2012, **73**, 261–284.
95 Q. M. Wang, D. Shen, M. Bülow, M. L. Lau, S. Deng, F. Fitch, N. O. Lemcoff and J. Semanscin, *Microporous Mesoporous Mater.*, 2002, **55**, 217–230.
96 T. M. Nicholson and S. K. Bhatia, *J. Phys. Chem. B*, 2006, **110**, 24834–24836.
97 S. Wang, Q. Yang and C. Zhong, *Sep. Purif. Technol.*, 2008, **60**, 30–35.
98 (*a*) J. W. Yoon, I. T. Jang, K.-Y. Lee, Y. K. Hwang and J.-S. Chang, *Bull. Korean Chem. Soc.*, 2010, **31**, 220–223; (*b*) A. Wagener, M. Schindler, F. Rudolphi and S. Ernst, *Chem. Eng. Technol.*, 2007, **79**, 851–855.
99 M. Jorge, N. Lamia and A. E. Rodrigues, *Colloids Surf., A*, 2010, **357**, 27–34.
100 (*a*) N. Lamia, M. Jorge, M. A. Granato, F. A. AlmeidaPaz, H. Chevreau and A. E. Rodrigues, *Chem. Eng. Sci.*, 2009, **64**, 3246–3259; (*b*) A. F. P. Ferreira, J. C. Santos, M. G. Plaza, N. Lamia, J. M. Loureiro and A. E. Rodrigues, *Chem. Eng. J.*, 2011, **167**, 1–12.
101 (*a*) M. Hartmann, D. Himsl, S. Kunz and O. Tangermann, *Zeolites and Related Materials: Trends, Targets and Challenges, Proceedings of 4th International FEZA Conference*, 2008, 615–618; (*b*) M. Hartmann, S. Kunz, D. Himsl and O. Tangermann, *Langmuir*, 2008, **24**, 8634–8642.
102 J. W. Yoon, Y.-K. Seo, Y. K. Hwang, J.-S. Chang, H. Leclerc, S. Wuttke, P. Bazin, A. Vimont, M. Daturi, E. Bloch, P. L. Llewellyn, C. Serre, P. Horcajada, J.-M. Grenèche, A. E. Rodrigues and G. Férey, *Angew. Chem., Int. Ed.*, 2010, **49**, 5949–5952.
103 Z. Bao, S. Alnemrat, L. Yu, I. Vasiliev, Q. Ren, X. Lu and S. Deng, *Langmuir*, 2011, **27**, 13554–13562.
104 Y.-S. Bae, C. Y. Lee, K. C. Kim, O. K. Farha, P. Nickias, J. T. Hupp, S. T. Nguyen and R. Q. Snurr, *Angew. Chem., Int. Ed.*, 2012, **51**, 1857–1860.
105 S. Uchida, R. Eguchi, S. Nakamura, Y. Ogasawara, N. Kurosawa and N. Mizuno, *Chem. Mater.*, 2012, **24**, 325–330.
106 K. Li, D. H. Olson, J. Seidel, T. J. Emge, H. Gong, H. Zeng and J. Li, *J. Am. Chem. Soc.*, 2009, **131**, 10368–10369.
107 C. Y. Lee, Y.-S. Bae, N. C. Jeong, O. K. Farha, A. A. Sarjeant, C. L. Stern, P. Nickias, R. Q. Snurr, J. T. Hupp and S. T. Nguyen, *J. Am. Chem. Soc.*, 2011, **133**, 5228–5231.
108 (*a*) C. Gücüyener, J. v. d. Bergh and J. Gascon, *J. Am. Chem. Soc.*, 2010, **132**, 17704–17706; (*b*) J. v. d. Bergh, C. Gücüyener, E. A. Pidko, E. J. M. Hensen, J. Gascon and F. Kapteijn, *Chem.–Eur. J.*, 2011, **17**, 8832–8840.
109 H. Järvelint and J. R. Fair, *Ind. Eng. Chem. Res.*, 1993, **32**, 2201–2207.
110 (*a*) H. Bux, C. Chmelik, R. Krishna and J. Caro, *J. Membr. Sci.*, 2011, **369**, 284–289; (*b*) Y. Pan, T. Li, G. Lestari and Z. Lai, *J. Membr. Sci.*, 2012, **390–391**, 93–98; (*c*) J. Caro, *Curr. Opin. Chem. Eng.*, 2011, **1**, 77–83.
111 A. Motelica, O. S. L. Bruinsma, R. Kreiter, M. d. Exter and J. F. Vente, *Ind. Eng. Chem. Res.*, 2012, **51**, 6977–6986.
112 A. Anson, Y. Wang, C. C. H. Lin, T. M. Kuznicki and S. M. Kuznicki, *Chem. Eng. Sci.*, 2008, **63**, 4171–4175.
113 (*a*) J. A. Mason, K. Sumida, Z. R. Herm, R. Krishna and J. R. Long, *Energy Environ. Sci.*, 2011, **4**, 3030–3040; (*b*) Z. R. Herm, R. Krishna and J. R. Long, *Microporous Mesoporous Mater.*, 2012, **157**, 94–100; (*c*) R. Krishna, *Microporous Mesoporous Mater.*, 2012, **156**, 217–223; (*d*) R. Krishna and J. M. van Baten, *Sep. Purif. Technol.*, 2012, **87**, 120–126.
114 (*a*) D. M. Ruthven and S. C. Reyes, *Microporous Mesoporous Mater.*, 2007, **104**, 59–66; (*b*) R. Krishna and J. M. van Baten, *Microporous Mesoporous Mater.*, 2011, **137**, 83–91.
115 C. Chmelik, J. van Baten and R. Krishna, *J. Membr. Sci.*, 2012, **397–398**, 87–91.
116 C. Zhang, Y. Dai, J. R. Johnson, O. Karvan and W. J. Koros, *J. Membr. Sci.*, 2012, **389**, 34–42.
117 H. W. Dandekar, G. A. Funk and H. A. Zinnen, *U.S. Pat*, 2000, US6069289A.
118 (*a*) T. Maesen and T. Harris, *U.S. Pat*, US70374222, 2006; (*b*) T. Maesen and T. Harris, *U.S. Pat*, US7029572, 2006.
119 P. S. Bárcia, F. Zapata, J. A. C. Silva, A. E. Rodrigues and B. Chen, *J. Phys. Chem. B*, 2007, **111**, 6101–6103.
120 Y. Ling, Z.-X. Chen, F.-P. Zhai, Y.-M. Zhou, L.-H. Weng and D.-Y. Zhao, *Chem. Commun.*, 2011, **47**, 7197–7199.
121 P. S. Bárcia, D. Guimarães, P. A. P. Mendes, J. A. C. Silva, V. Guillerm, H. Chevreau, C. Serre and A. E. Rodrigues, *Microporous Mesoporous Mater.*, 2011, **139**, 67–73.
122 H. J. Choi, M. Dincă and J. R. Long, *J. Am. Chem. Soc.*, 2008, **130**, 7848–7850.
123 R. Krishna and J. M. van Baten, *Phys. Chem. Chem. Phys.*, 2011, **13**, 10593–10616.
124 L. Pan, D. H. Olson, L. R. Ciemnolonski, R. Heddy and J. Li, *Angew. Chem., Int. Ed.*, 2006, **45**, 616–619.
125 L. Alaerts, M. Maes, M. A. v. d. Veen, P. A. Jacobs and D. E. De Vos, *Phys. Chem. Chem. Phys.*, 2009, **11**, 2903–2911.
126 M. Maes, L. Alaerts, F. Vermoortele, R. Ameloot, S. Couck, V. Finsy, J. F. M. Denayer and D. E. De Vos, *J. Am. Chem. Soc.*, 2010, **132**, 2284–2292.
127 D.-J. Lee, Q. Li, H. Kim and K. Lee, *Microporous Mesoporous Mater.*, 2012, **163**, 169–177.
128 X. Zhao, D. Sun, S. Yuan, S. Feng, R. Cao, D. Yuan, S. Wang, J. Dou and D. Sun, *Inorg. Chem.*, 2012, **51**, 10350–10355.